DESIGN OF A PROPRIOCEPTIVE ACTUATOR UTILIZING A CYCLOIDAL GEARBOX

A Thesis

presented to

the Faculty of California Polytechnic State University,

San Luis Obispo

In Partial Fulfillment

of the Requirements for the Degree

Master of Science in Mechanical Engineering

by

Craig John Kimball

June 2022

COMMITTEE MEMBERSHIP

TITLE:	Design of a Proprioceptive Actuator Utilizing a Cycloidal Gearbox
AUTHOR:	Craig John Kimball
DATE SUBMITTED:	June 2022
COMMITTEE CHAIR:	Siyuan Xing, Ph.D. Assistant Professor of Mechanical Engineering
COMMITTEE MEMBER:	Charlie Refvem, M.S. Lecturer for Mechanical Engineering
COMMITTEE MEMBER:	Eric Espinoza Wade, Ph.D. Assistant Professor of Mechanical Engineering

ABSTRACT

Design of a Proprioceptive Actuator Utilizing a Cycloidal Gearbox

Craig Kimball

Legged robotics creates the demand for high torque compact actuators able to develop high instantaneous torque. Proprioceptive actuator design theory is a design theory that removes the need for a torque feedback device and relies on the stiffness in the leg for absorbing the high Ground Impact Forces created by walking locomotion. It utilizes a high torque density motor paired with a gearbox with a high gear ratio for torque multiplication. Previously work has been done to design a proprioceptive actuator design that utilizes a planetary gearbox to create a modular low-cost actuator for legged robotics. The purpose of this thesis is to design and analyze a proprioceptive actuator that utilizes a cycloidal gearbox design to test the feasibility of the gearbox design and look at the advantages it might bring over a planetary gearbox design. A cycloidal gearbox utilizes eccentric motion of cycloidal disks, made of epicycloids, to create a high gear ratio in a very limited space without having to rely on expensive gears for torque multiplication purposes. A prototype low-cost actuator was developed using a 2-disk cycloidal gearbox in its design. It was tested for wear life and torque control and was able to meet the torque and operation requirements of the Cal Poly legged robotics project. The design was also optimized to be made using low-cost additive manufacturing techniques rather than relying on conventional machining.

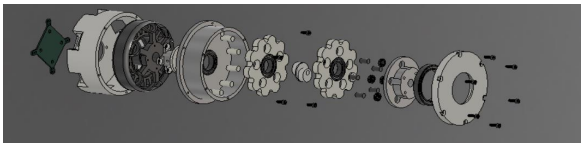

Keywords: Robotics, Cal Poly Legged Robotics, Actuator, Cycloidal Gearbox, Gearbox, Cycloid, Proprioceptive, Legged Robotics, Quadruped

ACKNOWLEDGMENTS

I would like to thank my family for providing support and motivation throughout my entire college career. I would like to thank my advisors, for being willing to meet with me weekly to make sure my project was going well and provide me with resources and advice whenever I had issues.

TABLE OF CONTENTS

LIST OF TABLES

LIST OF FIGURES

Figure Page

1.0 INTRODUCTION

Legged robots are beginning to be used in the world for carrying gear across uncontrolled terrain and have shown great potential in the field of search and rescue. The actuators used in these designs must be able to provide high instantaneous torque and fit in the often-narrow chassis of quadruped robots. The purpose of this thesis is to design and analyze a new modular actuator system for the Cal Poly Legged Robotics platform. One of the foci of this platform being developed by Cal Poly is specifically on jumping motion and jumping kinematics. Jumping is a complex motion that exhibits very strong reaction forces through the knees and hips in quadrupeds and is very difficult to simulate in robotics. Currently, there are few off the shelf options to purchase in terms of motors and actuators designed for use in quadruped robots based on work done on the MIT Cheetah platform which utilize a planetary gearbox. One of the major goals of this project is to determine if any of these alternatives are more cost effective in small quantities and better suited for use in a robot focused on legged jumping locomotion. I am analyzing the use of a novel gearbox design a cycloidal gearbox, in an actuator. The goal is to determine if there are any major performance advantage sin this gearbox design compared to traditional off the shelf models. Cost and modularity are an important factor in the design, as the team wants the actuator to be able to be used in future projects. This project is important as legged robots are one of the new emerging fields within the field of Mechanical Engineering and developing an affordable modular platform for Cal Poly to use provides a learning tool for future students in the design and control of legged robotics.

1.1 PURPOSE OF STUDY

The purpose of this thesis is to design and analyze the construction of a new novel proprioceptive actuator design using a cycloidal gearbox design. Based on the work done by Bradley Kwan in a previous thesis the actuator needs to be able to provide an instantaneous torque output of 7Nm [1]. This is the minimum torque required for the robot to achieve flight in jumping locomotion using the current weight of the prototype platform. The actuator design needs to be competitive in cost to other off the shelf actuators, and a target cost of $349 was set. This is cost was decided based on the cost of the current actuators used on the prototype platform. Work done in Ben Katz thesis for the MIT Cheetah actuator only considered cost of materials and did not include any manufacturing cost. This same assumption for cost is used in this project. This will reduce the overall cost of the design. Since the design is meant to be manufacturable in university shop facilities the cost of labor can be neglected.

2.0 LITERATURE REVIEW

2.1 PROPRIOCEPTIVE ACTUATORS

Legged Robotics is an emerging field of study focused on the design of robots able to navigate difficult and unstable terrain like a human or animal. In the last 4 years universities, and some companies like Boston Dynamics, have begun studying and improving the field. An important paper for this project is one written about the MIT Cheetah platform actuator titled “Proprioceptive Actuator Design in the MIT Cheetah: Impact Mitigation and High-Bandwidth Physical Interaction for Dynamic Legged Robots”. This paper analyzed the use of high-gap radius rotors in motor design to achieve higher torque density in the motor to create a smaller actuator package for legged robotics. One of the 3 factors that makes up proprioceptive actuator design. Legged locomotion involves repeated dynamic interactions with the environment and instant moments of high loading in opposing direction of actuator rotation. [2] Proprioceptive actuation is a proposed solution to this problem in which the actuator design philosophy is switched to focus on factors that relate specifically to legged locomotion like impact mitigation and instantaneous torque control [2]. A generalized proprioceptive actuator design concept is shown in the figure below.

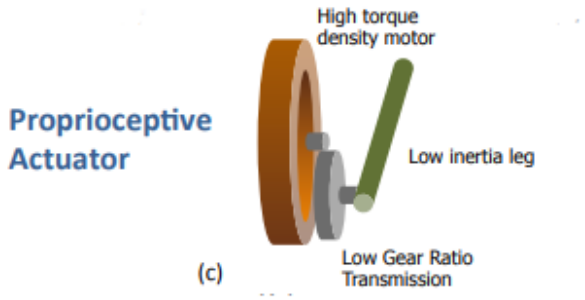

Figure 1: Proprioceptive Actuator Generalized Design

In this design there is no exteroceptive sensor for providing sensory feedback for torque control. All the actuator control and modulation are handled by a torque controller

connected to the high torque density motor. This reduces the number of components in the design and improves contact stability [2]. This design has been used successfully in previous projects like the pHANToM Haptic Interface [3]. This device measured the user's fingertip position and applied a specified force vector back onto the finger using a proprioceptive actuator design to allow the user to "feel" a virtual object. To reduce cost and space of the design actuators were designed that used minimal external sensors for feedback to a controller and relied primarily on torque control to the input motor.

2.2 CHALLENGES IN ACUTATOR DESIGN FOR LEGGED ROBOTICS

When designing an actuator for legged robotics there are multiple issues that must be addressed to create a sufficient design. These can be simplified into a few categories, Torque Density, Efficiency, and Impact Mitigation. Torque Density is a metric that relates actuator mass to the high torque output [2]. It is critical for running robots that the actuator have a high torque density. This is due to the high ground reaction forces (GRF) required for movement [2]. During motion each time the leg strikes the ground it is treated as an impact force, which transfers significantly higher loads through a leg than the normal forces experienced when standing. In a study on dogs, it was found that GRF were found to be 2.6-2.8 times the bodyweight of a dog during a gallop of 9m/s [4]. This means that increasing actuator size to meet torque demands is not a good design choice. As actuator size increases so will its mass meaning the GRF forces on impact will also increase so no benefit is gained. Instead, designing to maximize torque density is a better way to optimize the actuator design

Energy efficiency is another important metric in evaluating the design of an actuator for legged robotics. In the actuation of the leg there are 3 main energy losses that can be observed; Joule heating, transmission loss, and interaction losses. [5] Joule heating is a

heat energy loss created by the motor when the actuator needs to generate high torque. Transmission losses come from inertial and friction-based losses in the gearbox of the actuator. These 2 losses can be observed as being inversely related. As you reduce the gearing ratio in the gearbox, transmission losses in the gearbox are reduced at the cost of creating more joule heating from the higher torque requirement needed from the motor. Similarly, as the gear ratio in the gearbox increases the friction and inertia in the transmission increase, creating higher losses in the transmission, but a lower torque demand from the motor. Modeling the energetics of gears accurately is a very complicated task [2] so it is more efficient to consider this inverse relationship of losses as a guideline for design rather than setting strict requirements. Interaction losses come from interaction of the leg with the ground surface and will not be considered in the design of this actuation system. Instead focus will also be put into impact mitigation. Impact Mitigation refers to the legs ability to mitigate the high GRFs created during ground collision. In prior designs for legged robotics this was handled by impedance control from the motor, using force sensors along the legs to measure the impact force [2]. In proprioceptive actuator designs, mechanical solutions like compliance in the legs, or back driving of the actuator serve as the absorption techniques used to absorb the transmitted impact forces through the leg [2].

2.3 MIT CHEETAH PLATFORM

One of the first actuator designs for legged robotics that utilized proprioceptive actuator theory was one for the MIT Cheetah III platform developed by Ben Katz in his thesis project “A Low-Cost Modular Actuator for Dynamic Robots”. This design was created to be a modular actuator for use in any low impact legged robotics platform, and because it has been published through MIT has influenced most of the currently available off the shelf actuator designs for legged robotics that we see today. This design utilizes a planetary gearbox, with a 10:1 gear ratio and an inexpensive hobby plane motor. It relies on many of the shelf parts to make up the planetary gearbox system and modifying the motor to seat the ring gear inside the stator frame of the motor. The design was optimized to try to reduce machining operations needed on each part to simplify manufacturing and improve the accuracy and precision in the tolerances for the critical components of the design. To reduce the packaging envelope of the design a motor was selected that allowed for modification of the rotor by mounting the external ring gear of the planetary reducer directly on the motor. This put the planetary gearbox and motor inline within the actuator making for very efficient packaging of the actuator components. The motor selected was based on parameterization work done by Benjamin Katz in which multiple motors were compared and characterized in a one-legged robot system [6]. A custom motion board was also developed that focused on utilizing minimal space in the rear of the actuator while providing Torque and Impedance control for a low impedance planetary gearbox [6].

Figure 2: MIT Cheetah III Actuator Designed by Ben Katz [7]

The benefits of this gearbox design are that it is very easy to manufacture, and that the gearbox has very low backlash, making the system response time much faster in torque control [7].

Table 1: Ben Katz Actuator Specifications [7]

Mass	480g
Dimensions	96mm O.D, 40mm axial length
Maximum Torque	17Nm
Continuous Torque	6.9Nm
Maximum Output Speed	40rad/s @ 24v
Maximum Output Power	+250/-680 watts
Output Inertia	0.0023kgm^2

2.4 CYCLOIDAL DRIVE GEARBOX

One of the goals of my thesis was to look into alternative gearbox designs for the actuator. For torque multiplication purposes other gearbox designs that could be used are a cycloidal drive, harmonic drive, or conical drive. A cycloidal drive gearbox is a gearbox design that relies on an offset cycloidal disk to create the torque multiplication from the input to the output. An example of an explode view cycloidal gearbox is shown below.

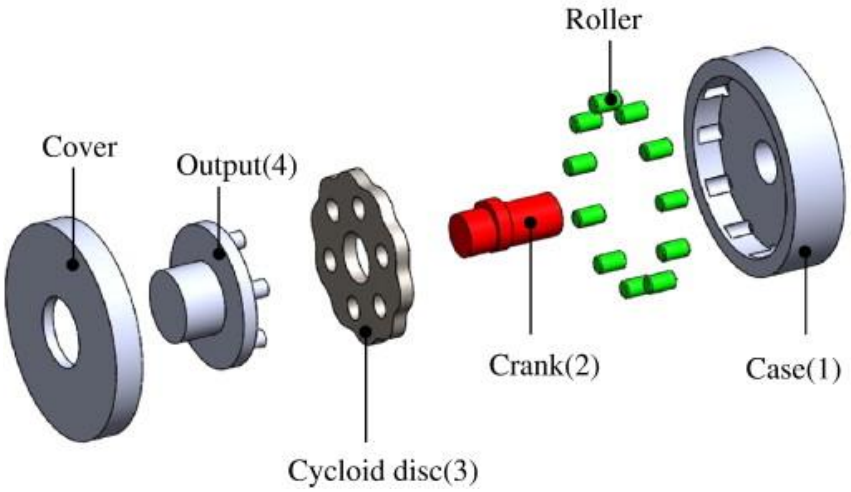

Figure 3: Exploded View of Simplified Cycloidal Drive [8]

The gearbox contains 4 major components. The main component being the cycloidal disk which rotates in an eccentric motion due to being mounted on an offset input shaft. This eccentric motion pushes the pins on the output disk converting the eccentric rolling about the outer roller pins into a pure rotational motion about the center of the gearbox. The ratio of the number of waves along the outer profile of the cycloidal disk to the number of rollers along the case determines the “gear ratio” or the torque multiplication constant of the gearbox. One of the advantages of this gearbox design is it does not use traditional gears, which are difficult to manufacture in a university setting and expensive to buy off the shelf from a vendor. Since the cycloidal disk can be custom designed it gives greater control to the designer to control the exact torque multiplication constant

that the gearbox creates. A main constraint of this design is it relies on the use of ball bearings, and so the thickness of certain components like the cycloidal disk or input shaft are limited to the available sizes of ball bearings. At higher speeds a cycloidal gearbox using a single disk design can induce higher vibration that a planetary equivalent.

3.0 GEARBOX DESIGN

3.1 GEARBOX DESIGN CHOICE

One of the first steps in accomplishing this project was selecting the gearbox design philosophy that would be used for the actuator system. The table below lists out the high-level requirements for actuator design selection

Table 2: High Level Actuator Design Specifications

Mass	>500g
Size	96mm OD, 40mm axial length
Max Torque	7Nm
Cost	>$349.99

Looking at the requirements for the actuator it was clear that the cost and dimensions of the actuator would be the 2 constraining factors of the design. Another important feature of the gearbox design would be the ability to reliably manufacture multiple units using conventional machining techniques, and ideally something Cal Poly could use its on-campus shops to manufacture in the future. With these ideas in mind the first step taken in deciding what gearbox platform I would use was to design some basic prototypes of each to get an idea of what will be better for the final design.

3.1.1 PLANETARY GEARBOX

The main constraint of the development of the Planetary gearbox came from the commercially available selection of internal spur gears, which would be used as the output ring for the gearbox. Due to supply shortages resulting from the Covid 19 pandemic there was some limited selection of internal spur gears due to size and cost restrictions. For the design a internal spur gear was selected which had an external diameter of 75mm and an internal diameter of 60mm measured at the tooth top face. The gear had a module of 1.5 and 100 teeth. The face width of the gear would be machined down from the stock 8mm to 4mm to help reduce the overall thickness of the gearbox. For the internal sun and planet gears, to reduce cost and simplify the design, 30 tooth gears were selected to mate with the internal spur gear. A model of the gearbox is shown below.

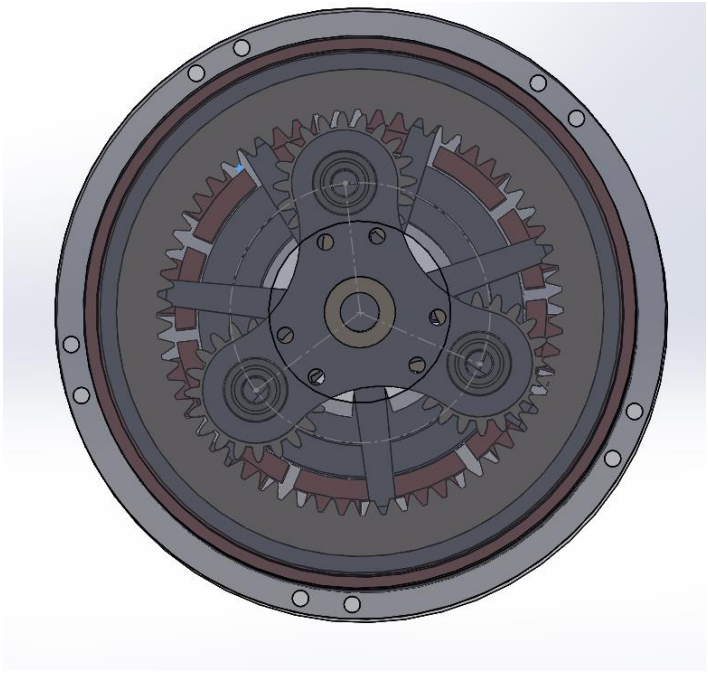

Figure 4: Prototype Planetary Gearbox Design

This gave a torque multiplication constant of 3.0 shown by the calculation below.

$$\text{Gear Ratio} = \frac{T_2}{T_1}$$

$$T_2 = \text{Number of teeth in output gear}$$

$$T_1 = \text{Number of teeth in input gear}$$

$$\frac{100}{30} = 3.0$$

To meet the 7Nm output torque requirement of the platform this means the motor used for this gearbox will need to provide an input torque of at least 2.5Nm. This limited the motor selection substantially and drove up the cost of the motor to find one that would be able to meet the parameters needed. This coupled with the high cost of gears during the time this project was conducted are the reasons why I decided to use a different gearbox design.

3.1.2 CYCLOIDAL GEARBOX

The cycloidal gearbox prototype was designed trying to keep the outer diameter of the actuator package the same as Ben Katz actuator. For the design of the cycloidal gearbox all custom components were designed to try to reduce the number of fixturing needed to manufacture a part if a CNC was needed, or to simplify printing in an additive manufacturing process.

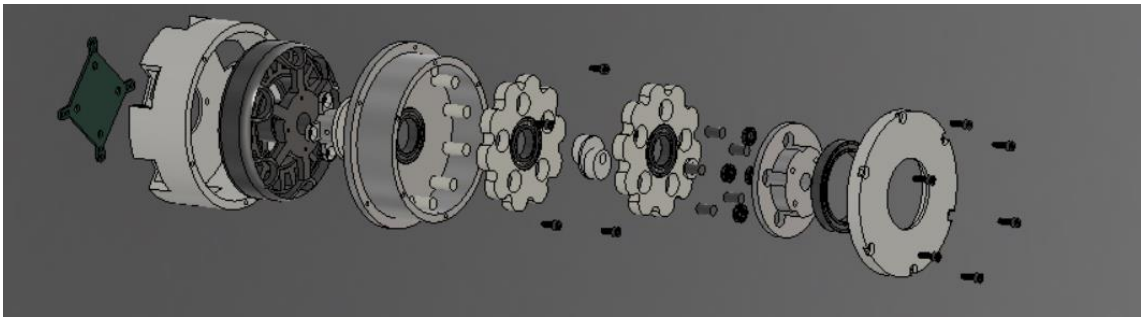

Figure 5: Cycloidal Gearbox Design

In the Figure 4 an exploded view of the gearbox is shown. All these components were designed to require as few machining operations as possible if subtractive machining operations were chosen for manufacturing. In recent years 3D printing using engineering grade materials has become far more cost effective and attainable in a consumer and university setting and utilizing additive manufacturing, the cost of the unit can be further reduced. This also allows for designs to be more complex without increasing manufacturing complexity. In the cycloidal gearbox design components that are of the shelf are limited to shafts and bearings, which are much cheaper per part than gears. The gearbox design shown in Figure 4 has a 10:1 gear reduction ratio meaning that the torque multiplication constant is 10, considerably higher when compared to the 3.0 constant from the planetary system. Below is a cost table for the actuator design shown in Figure 4.

Table 3: Cost Table for Cycloidal Gearbox Prototype

Item	Qty	Cost per unit	Cost
Gearbox Housing	1	$48.87	$48.87
Motor Housing	1	$2.43	$2.43
M3x0.5 10mm screw	6	$0.11	$0.66
M3x0.5 8mm screw	5	$0.11	$0.55
40mm ID, 52mm ID Bearing	1	$27.70	$27.70
1556 Carbon Steel 6mm OD shaft, 200mm	1	$8.11	$8.11
6mm ID, 10mm OD Bearing	6	$27.17	$163.02
20mm ID, 32mm OD Sealed Bearing	1	$15.42	$15.42
17mm ID, 30mm OD bearing	2	$9.23	$18.46
6mm ID Nylon Washer	2	$0.67	$1.34
Neodymium magnet, magnetized through diameter 1/8" thick, 1/4" OD	1	$3.17	$3.17
Alloy steel cup-point M3 set screw	1	$0.06	$0.06
6mm Steel Retaining Ring	6	$0.07	$0.43
5/16" OD Delrin rod 5'	1	$4.20	$4.20
Output Disk	1	$0.75	$0.75
Cycloidal Disk	2	$0.67	$1.34
Eccentric Spacer	1	$0.05	$0.05
EaglePower 8308 motor	1	$65.08	$65.08
AMS 5147 Eval Board	1	$30.38	$30.38
Motion Board	1	$62.80	$62.80
	Total:	**$307.05**	**$454.82**

In the Table above a cost breakdown is given for the gearbox prototype built and tested in this thesis. For 3D printed components the cost was estimated by looking at the cost per gram for material. Electrical costs for running the printer were not considered. For the metal gearbox housing the cost only includes cost of material, not cost of labor or electricity. All parts were manufactured by me, so cost of labor was neglected. Due to part shortages caused by the Covid-19 pandemic cost of some components varied considerably during the duration of this thesis. Bearing prices were especially volatile with the price of the 10mm bearings used in the output disk increasing in price by 100%

during the time they were purchased. The final robot will need 8 actuators to perform the jumping motion simulated, so by using less expensive off the shelf parts, like gears, and relying more on manufacturing in the Cal Poly shops or the use of additive manufacturing helps reduce the overall cost of the actuator system and gives it potential to be a modular package that could be used in future Cal Poly projects. I also believe that further optimization can be done on motor choice and packaging to reduce the length of the package.

3.2 DESIGNING THE GEARBOX

3.2.1 CYCLOIDAL DISK

The critical component of any cycloidal gearbox design is the cycloidal disk. It is what performs the torque multiplication in the system and experiences the highest loads during operation. The outer profile of the cycloidal disk is a cycloidal curve, which is what will use the eccentric motion to develop the gear reduction. To develop the cycloidal disk geometric equations were used. The first step was deciding on a pin size for the cycloid and the gear ratio. This will determine the diameter of the cycloidal profile and influence the eccentricity radius of the disk. Based on the size limitations of the gearbox a 7mm pin was selected for the cycloidal frame, and in order to minimize the power of the motor needed a 10:1 gear reduction ratio was selected. Given these 2 parameters the diameter of the cycloidal disk was calculated using:

$$\text{Disk Diameter} = \text{Pin Size} \times \text{Gear Reduction Ratio}$$

$$7\text{mm} \times 10.0 = 70\text{mm}$$

Once the diameter of the cycloidal profile was determined the next step was to develop the cycloidal spline of the disk. This is done by mapping a singular point along the outer pin, as it rotates along the diameter of the cycloidal profile. This was done in Fusion 360

as Fusion allows you to translate shapes along tangent edges in a sketch making it easy to use a construction circle to map the cycloidal spline. This mapping is done by specifying the angle of rotation of the outer pin with reference to the angle of a point to the radius of the cycloidal profile. The setup is shown below.

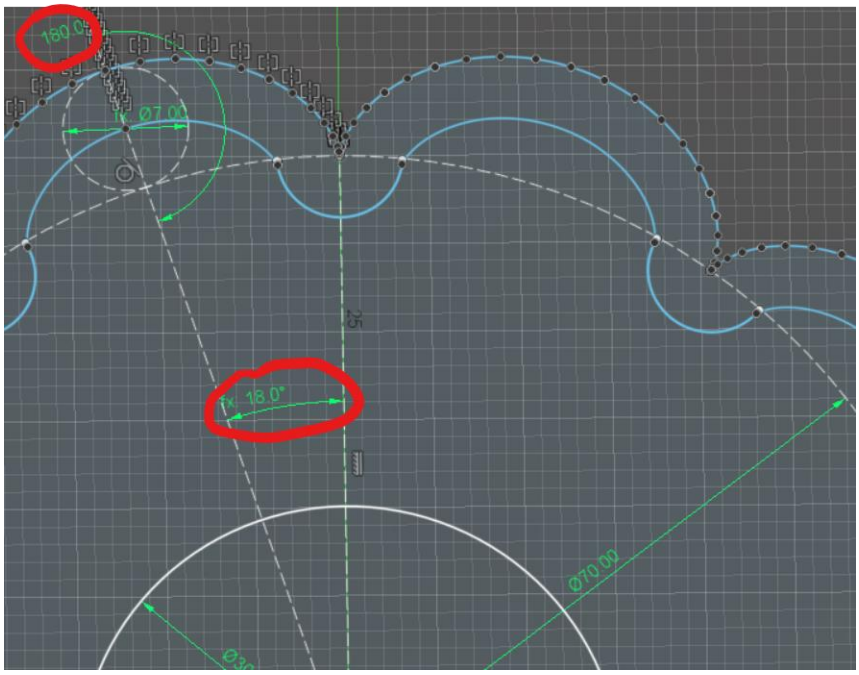

Figure 6: Development of Cycloidal Profile

In Figure 4 the angle of the point on the outer pin is at 180 deg. The equation used to calculate the angle of the outer pin on the cycloidal disk diameter is given below:

$$\theta = \text{Outer Pin Angle} / \text{Gear Reduction Ratio}$$

This gives an outer pin angle in this case of 18 deg. Now when the angle of the point on the outer pin is changed, the outer pin circle rolls along the cycloidal disk diameter mapping the cycloidal profile of the disk. You can see in Figure 4 the mapping of these points along the circle represented by all the black dots on the outer profile. The outer pin was rolled across 180 deg and then the profile created was patterned in Fusion to

create the full profile This is the theoretical profile of the cycloidal disk. This generated profile was then offset by the radius of the outer pins, 3 mm, to create the final cycloidal disk spline which is seen as the light blue spline pattern in Figure 4. This gives a cycloidal spline that will mesh well with the selected output pins and can easily be tweaked by adjusting the offset from the original profile to account for any tolerance specifications needed in manufacturing. This offset profile is known as the working profile. The working profile brings the midpoint of the cycloidal curve back in line with the pitch circle to ensure the cycloidal disk mates with the outer pin ring properly [9].

3.2.1.2 EPICYCLOID CURVE

An epicycloid is a curve produced by tracing the path generated by a chosen point on a circle called an epicycle [9]. The epicycle is rolled about another circle without slipping creating a parametric spline curve. In geometry there are 3 types of epicycloids possible: normal, shortened, and extended [10]. Extended is ignored as it is not practical in the use of developing a cycloidal gear profile. In a normal epicycloid the epicycle is rigidly connected to perimeter of the rolling circle by the radius of the rolling circle. This is what is shown above in Figure 5. For a shortened epicycloid the point followed lies within the perimeter of the rolling circle along a fixed radius where, the radius of the epicycle point is less than the radius of the rolling circle [9].

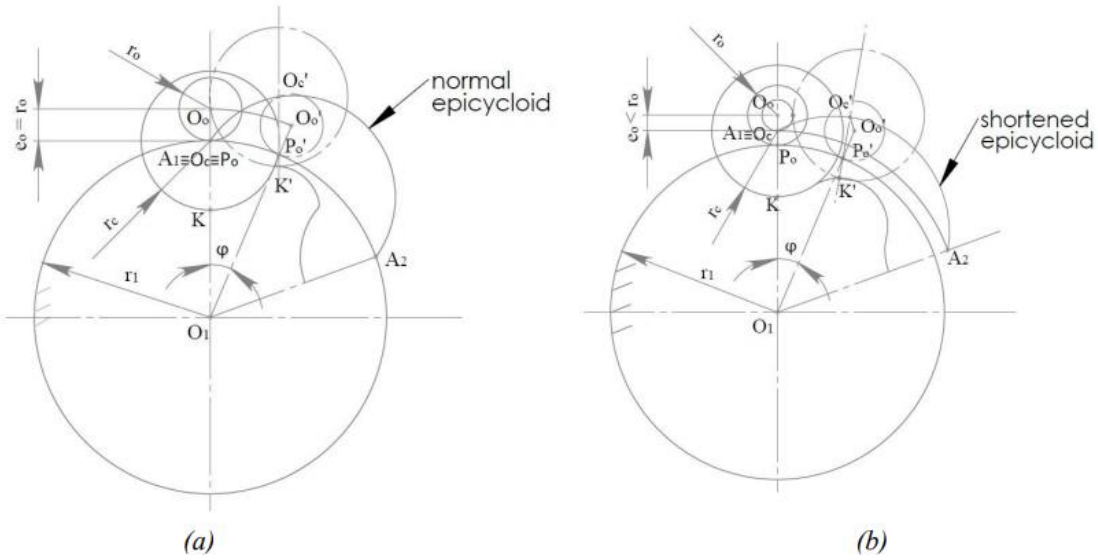

Figure 7: The Geometric Setup for a Normal and Shortened Epicycloid [10]

Table 4: Definition of Variables used in Figure 6

Symbol	Definition
r_o	Radius of Epicycle
e_o	Epicycloids epicycle
r_c	Outer Pins radius
φ	Angle of rotation of epicycle
r_1	Pitch Circle Radius

In the Figure and Table above, we can see how the epicycloid is developed from the epicycle rotating about the pitch circle. In the development of the cycloidal gear for the actuator these variables are defined by the outer pin size and overall actuator outer diameter. By fixing all the variables aside from φ and then recording the epicycle location at increments of φ an approximated epicycloid could be produced to define the profile of the cycloidal gear. In the Figure the point O_c' represents the point being tracked for developing the epicycloid. For the profile of the cycloidal disk used for this actuator that point was placed on the edge of the epicycle circle with $r_o = r_c$. This means a normal epicycloid was formed.

A cycloidal gear has both a theoretical and a working gear profile. The theoretical profile is used to generate the actual working profile by offsetting the theoretical profile by a distance equal to the radius of the working outer pin. This can also be seen in Figure 6 where the profile is offset 3.5mm to create the working profile. CAD programs make it much easier to develop a normal epicycloid profile by allowing the ability to roll a construction circle around the large profile circle to create the theoretical profile. Additionally, it allows the ability to introduce a parametric relationship between the epicycloid and the eccentricity of the system making it very easy to vary the theoretical and working profile of the cycloidal gear based on the eccentricity of the system. Fusion 360 allows the use of construction lines and circles, which is what has to plot points of the epicycloid curve by creating an equation-based dimensions to control the generation of the theoretical profile. For ensuring that a cycloidal disk meshes properly with the outer pins certain criteria must be met.

1. The radius of the circle for the placement of the outer pins, r_c is equal to $r_{1,}$ the pitch circle radius.
2. The difference between the number of pins and the number of “teeth” is equal to 1.

3. The distance between the center of r_c and the center of the cycloidal disk must be equal to the eccentricity of the design.

Each of these criteria ensure that the depth, height, and width of the lobes and concave pockets on the cycloidal disk are sized properly to accommodate the pin during motion and that the pins will mesh properly with the cycloidal disk during motion. The shape and profile of these disks can still be modified by shifting parameters that will be discussed below.

3.2.1.3 ECCENTRICITY

Eccentricity in a cycloidal disk or gear refers to the distance along a radius from the center of the disk to the point it is driven.

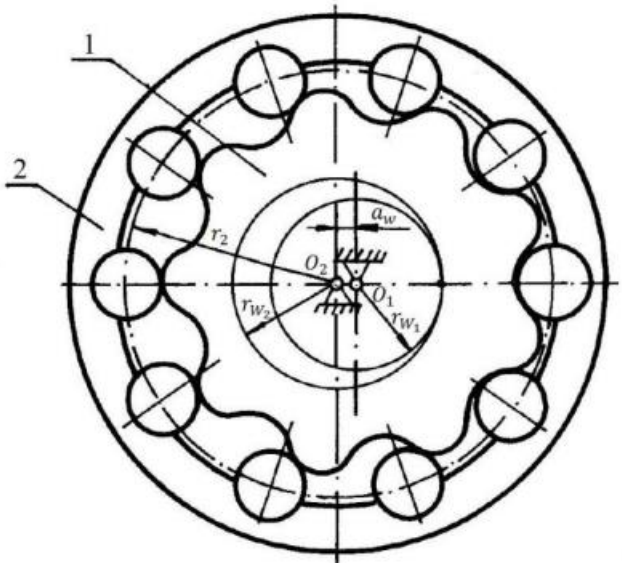

Figure 8: Eccentricity of a Cycloidal Disk in a Cycloidal Gearbox [10]

In Figure 8 point 0_2 represents the center of the gearbox and 0_1 represents the center of the cycloidal disk. The distance between these 2 points is the eccentricity of the system. The farther away this point is from the center the more eccentricity Is introduced into the part. To relate the design of the epicycloid to the eccentricity of the disk some

standardization of parameters of the gears must be introduced. This standardization allows us to think of the profile generation of the epicycloid as a tool like a rack cutter used for generating spur gears [9]. To use this tool a geometric reference circle referred to as a module circle must be introduced. The module circle is used as a base so that the parameters of the cycloidal disk and the profile cutting instrument are the same. The distance between the centers of the profile generating tool and the module circle is referred to as the system eccentricity, *e*. the eccentricity can be calculated using the equation:

$$e = \frac{m}{2}$$

where m is the module of the gear defined from the module circle. The module can be calculated using the circumference of the module circle also known as the pitch of the profile cutting instrument [10].

$$m = \frac{p}{\pi}$$

A visual representation of the eccentricity created by these 2 equations is shown in the figure below.

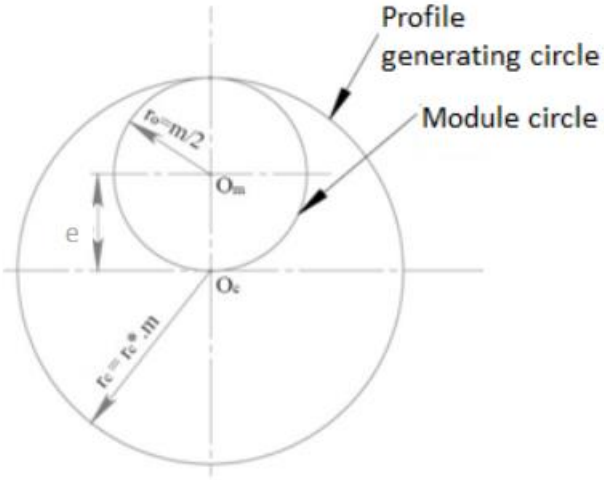

Figure 8: Profile Generating Contour [10].

With the eccentricity related to the generation of the profile cutting element we can then see how changing the radius of the profile cutting element will affect the tooth shape of our cycloidal disk. An example of this is shown in Figure 10.

3.2.1.4 GEAR MESHING

The cycloidal gear partially meshes with half of the outer pins at any one time. These pins are the load transmitting pins [10]. The transmitting angle between the disk and the meshed pins is based on the rotation of the outer housing relative to the cycloidal disk an angle defined as ψ. Using this angle, the angle of motion transfer [10], γ can be defined using an equation.

$$\gamma = \arcsin\left[\frac{(1-x)sin\psi}{\sqrt{1+(1-x)^2-2(1-x)cos\psi}}\right]$$

This equation is created from using the sin theorem on a triangle created from the center of the profile circle, the center of the outer pin, and a tangent point between the centrode circle of the epicycloid at this instance and the centrode circle of the outer pins. x is a variable called the Coefficient of Modification [9] and refers to the modification of the eccentricity from the max eccentricity calculated using the module circle and pitch circle.

Refer to the paper written by Hansson, Hans in the references for further description on this variable [9]. Simplifying this equation to find the maximum angle of transmission for the cycloidal disk gives the equation,

$$\gamma_{max} = \arcsin(1 - x)$$

A plot below shows how γ varies based on change in x and ψ.

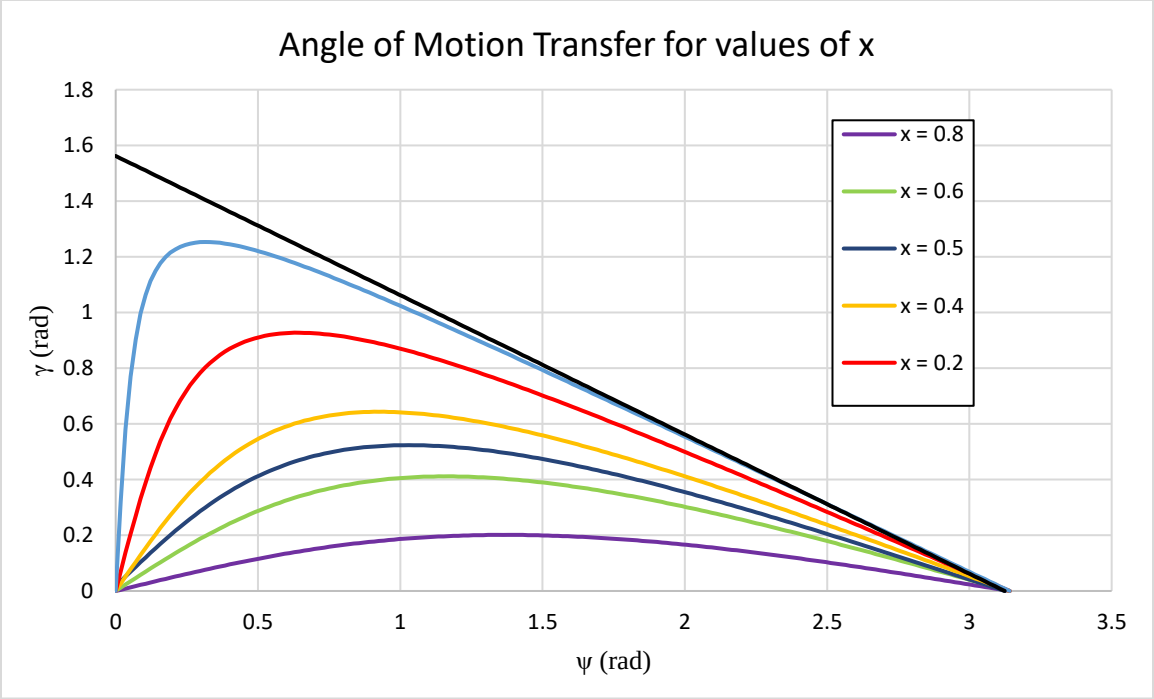

Figure 9: Plot Showing the Change in Angle of Motion Transfer Varying both x and ψ

In the Figure above you can see that for lower values of x a higher max angle of motion transfer is achieved. As x is increased then our teeth become shallower and less pronounced on the cycloidal disk which can be seen in Figure 10, as x is tied to eccentricity. For the design of the cycloidal disk in the prototype actuator the coefficient of modification was set to 0.5. The reason for this is discussed later.

3.2.2 ECCENTRIC SPACER

The next important part of the cycloidal disk gearbox is the eccentric shaft used to introduce the eccentric motion to the cycloidal disk. The radius of eccentricity is the radius from the center of the gearbox geometry to the center of the cycloidal disk geometry. This calculated by using the equation below.

$$\text{Eccentricity} = (\text{Diameter of outer pin}) / 2$$

This gives an eccentricity of 3.50mm for out design. This is different than using the equation utilizing the module circle. Because the outer pin diameter has already been defined, we can use this equation instead to solve for what the maximum eccentricity of this system can be rather than designing the pin placement and diameter based on a eccentricity calculated from the module circle. Minimizing the eccentricity radius helps reduce vibrations in the gearbox. This eccentricity was introduced into the cycloidal disk by use of eccentric spacer with an offset hole to accommodate the 6mm input shaft. By keeping the input shaft centered in the gearbox and using an eccentric spacer to create the eccentric motion it keeps more parts of the gearbox rotating about the center of geometry all to minimize vibration in the design. For the final version of this disk the eccentricity was backed off to 3mm. This was done to shallow out the mating interfaces of the cycloidal disk with the outer pins to reduce friction. As eccentricity is increased the concave mating points on the cycloidal disk become deeper and sharper, to accommodate for the larger diameter eccentric motion. By reducing this the transition between the concave and convex sections of the parametric profile become smoother and more gradual improving operation.

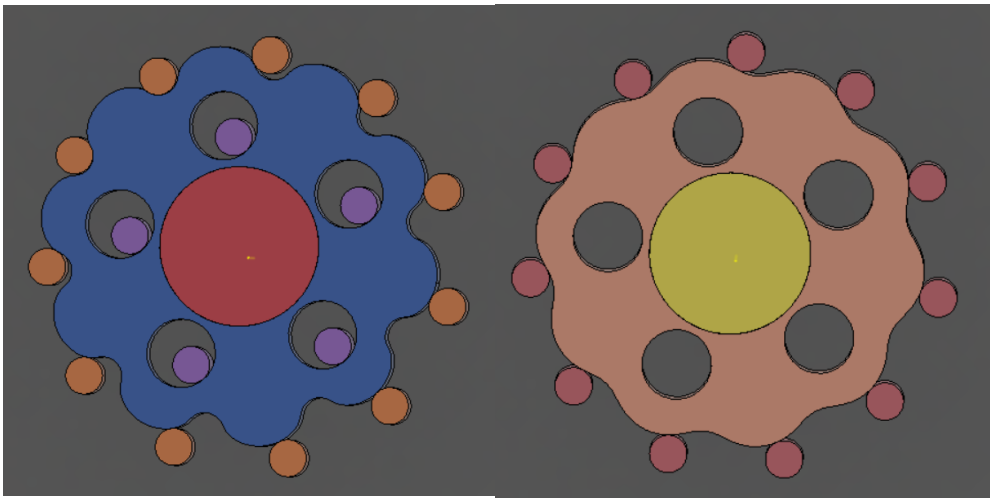

3mm eccentricity 2mm eccentricity

Figure 10: A Cycloidal Disk with 3mm of Eccentricity and 2mm of Eccentricity

In Figure 6 it is easy to see how changing the eccentric radius of the disk drastically effects the parametric profile of the cycloidal disk. With this considered the eccentric spacer designed was finalized below.

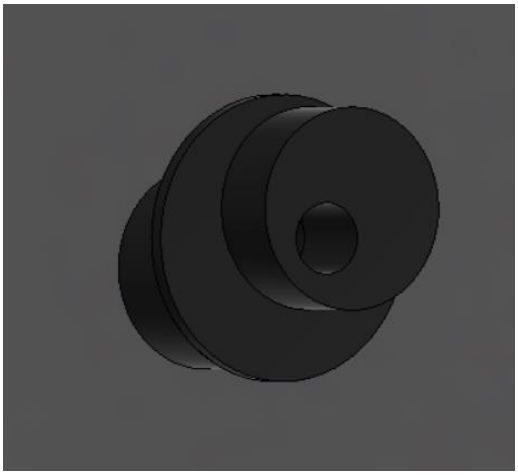

Figure 11: Joint Eccentric Spacer for 2 Cycloidal Disks

This component is one where I was unable to keep the manufacturing down to one operation using subtractive manufacturing techniques. Initially the design had been to have each disk have its own spacer, but it became hard to keep the phase of the 2 disks remain constant without adding set screws to the design complicating the part. By incorporating the offset of the 2 eccentric spacers, and then a thin wall to keep the disks from rubbing I can use a single component that can either be machined or 3d printed to introduce the eccentric motion into the cycloidal disks and keep them 180deg out of phase with each other.

3.2.3 OUTPUT DISK

The output disk in a cycloidal gearbox Is what translates the eccentric motion of the cycloidal disks back into a pure rotational motion. It is driven in this case by pins that stick into the holes on the cycloidal disk. As the cycloidal disk spins each pin will be pushed by the motion of the circles and will translate the motion back to pure rotational.

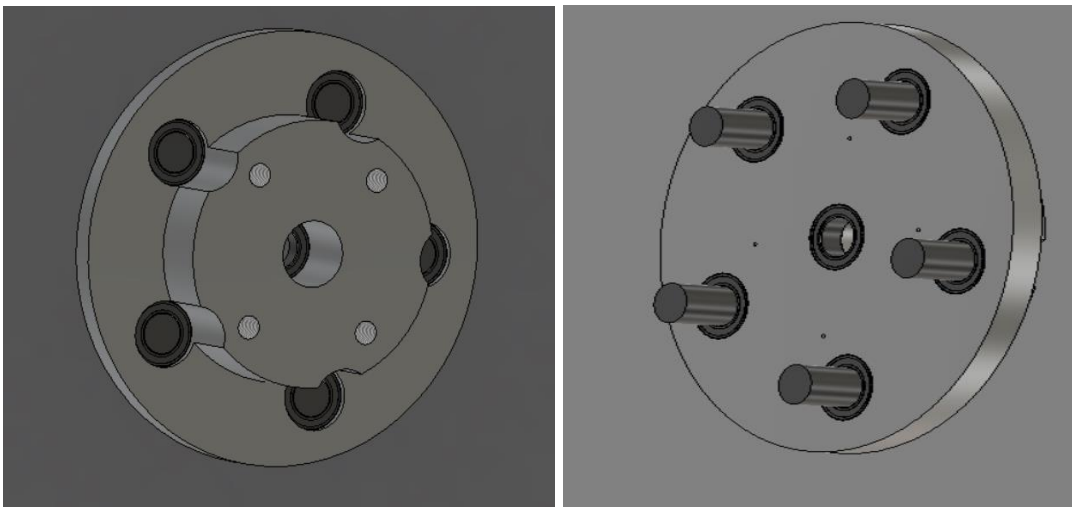

Figure 12: Top and Bottom Views of Output Disk for Cycloidal Gearbox

The dimension for both the holes on the eccentric disk and the diameter of the output holes on the output disk are related to each other through the following relationships.

$$OD_{E\ Disk} = \text{Diameter of Output Pin} + \text{Diameter of Eccentricity}$$

$$6mm + 7mm = 13mm$$

The spacing of the holes for the output pins on the output disk are set so that the pins sit along the inside edge of the output holes when both the output disk and cycloidal disk are centered. This is done so that the pins will always remain in contact with the cycloidal disk as it travels around its eccentric diameter, keeping backlash in the system to a minimal. It is also important from the requirements of this project that the gearbox be able to be back driven. By making sure the pins always contact a point in the gearbox, that means that in a five-pin arrangement, at any given point in the rotation 2 of the pins will be responsible for driving the disks in a back driving scenario. If the pins did not always contact the cycloidal disk, there is a risk of getting to a point where there is no pin able to drive the cycloidal disk due to there being a loss in contact or the pin contact being in the wrong place and unable to drive the motion. The pins are spaced 23mm from the center of the drive, such that they contact the far edge of the output holes. By making them contact the outside of the output holes, it gives a better moment arm for the robot arm to back drive the gearbox when it needs to. The farther away the pins can be along a radius from the input shaft, the easier it is to back drive the gearbox.

The output pins are slotted into roller bearings so that as they are pushed by the cycloidal disk, they roll around the internal circles reducing friction in the system. Mounting the bearings at the end of the pins as the contact surface that the cycloidal disk contacted was considered, but this would increase the holes in the cycloidal disk to

17mm which became too large to work with the cycloidal disk design without increasing the overall outer diameter of the gearbox.

The cycloidal disk then sits in a roller bearing in the top cover of the actuator assembly. This assembly is shown in Figure 13. The large output roller bearing is in purple, and the top cover is a transparent green so that the mating interface between output disk and cover can be seen. The output disk has a nylon spacer along its outer flange where it mates to the top cover. Initially it was proposed that a needle bearing would be used along the outer flange between the output disk and a thin top cover. However, solving for the resulting moments on the needle bearing and output disk for an out of plane force on the leg became very complex as it related to a change in stiffness and pressure along the bearing surface, so a roller bearing was used instead to simplify calculations. In future projects it is worth looking into the feasibility of using a thinner needle bearing to reduce cost and size of the actuator. This would reduce the cost and size of the design making the actuator fit into a tighter package.

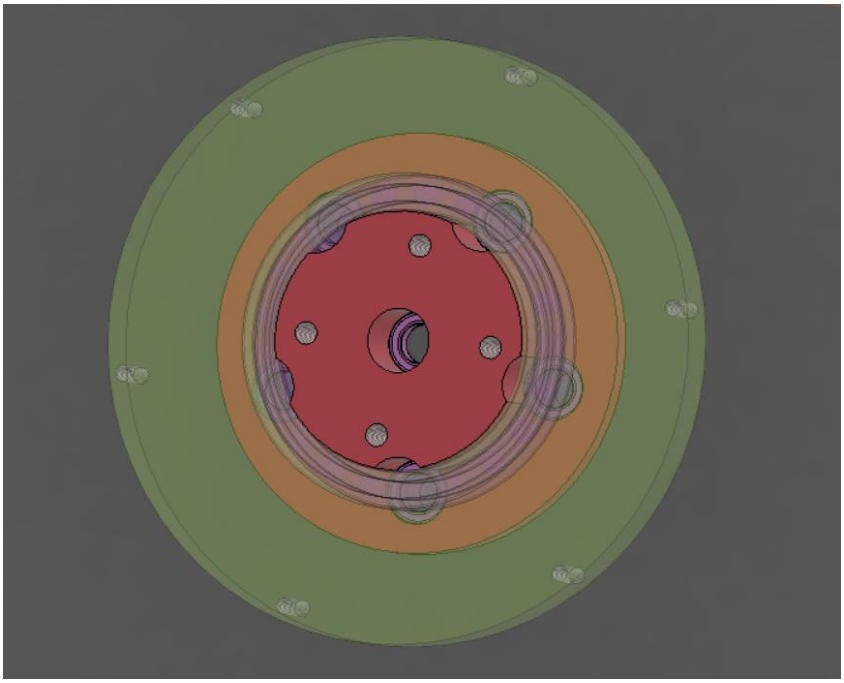

Figure 13: Top Cover and Output Disk Assembly

3.2.4 GEARBOX HOUSING

The housing contains all the components for the gearbox and acts as a mounting interface between the actuator and robot platform. The outer flange on bottom of the housing holds 5 clearance holes for M3 screws. These screws then screw into threaded holes in the motor housing and hold together the actuator as well as mounting it to the robot platform. The housing of the gearbox is made from T6-6061 Aluminum and is manufactured using a CNC mill. The housing was made of Aluminum to further dampen vibration in the system. Aluminum has a much higher density than Polycarbonate. This allows it to dampen some of the vibrations created by the gearbox in operation and make the operation quieter and smoother.

3.2.5 TWO DISKS VS. ONE DISK

A cycloidal drive gearbox contains a cycloidal disk rotating eccentrically about the center of the gearbox. This means that center of mass of the system shifts off center as the

cycloidal disk rotates. This introduces a lot of vibration into the system as the speed increases, since the center of mass of the cycloidal disk moves around the gearbox rather than remaining centered. to reduce the vibration in the system a second cycloidal disk was added into the design, that would sit 180° out of phase with the first cycloidal disk. With the two center of masses opposite of each other the effects of the vibration will be reduced as the gearbox's cg will remain centered about the rotating input shaft during operation. Additionally, by adding a second disk to the gearbox the loads experienced by each cycloidal disk between the disk and output shaft decreases. This force calculation is discussed in section 3.3. I believe in the future some vibration analysis work could be done on the gearbox design and the system could be simplified back to a singular disk, further simplifying the actuator design. Further work will need to be done on this.

3.2.6 MOTOR SELECTION

The gearbox was designed around the input shaft being able to input a minimum of 0.7Nm of torque to the gearbox. This is because the gearbox has a 10.0 torque multiplication factor. By reducing the input torque required it allowed for the use of lower powered brushless motors for the actuator which are often cheaper. Another important criterion for the motor was that it had to fit within a similar diameter enclosure of the MIT Cheetah platform which was 96mm. After researching various options, the EaglePower 8308 Brushless motor was found on Alibaba.

Figure 14: EaglePower 8308 Motor

The motor cost $65 per unit which was one of the lowest prices found during the search and more than $100 than a U.S made equivalent motor. The brushless motor has an outer diameter of 96mm, takes a 24V input, and can produce a maximum torque output of 1.2Nm. The motor had to be modified for use with the gearbox by using a cutoff wheel to remove the shaft head from the top of the motor to mount the mating piece from the motor to the input shaft. The input shaft was created based on the hole pattern on the motor and is used to drive the 6mm input shaft for the gearbox.

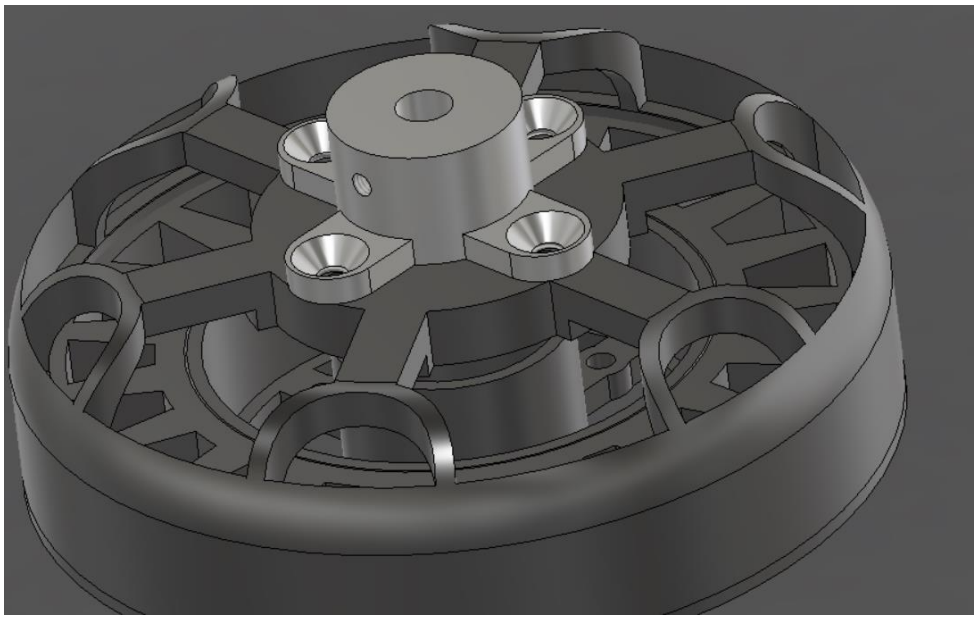

Figure 15: Motor Mount of Gearbox Input Shaft

3.2.7 MOTOR HOUSING

The design of the motor housing was created to serve 3 main functions. First to tie the Aluminum gearbox housing, and the motor/encoder assembly together into a single actuator unit. Second the housing needed to allow for proper ventilation such that the motor does not overheat during long periods of demanding operation. Finally, the housing needs to have mounting points for a magnetic encoder. These parameters led to the design shown in the figure below.

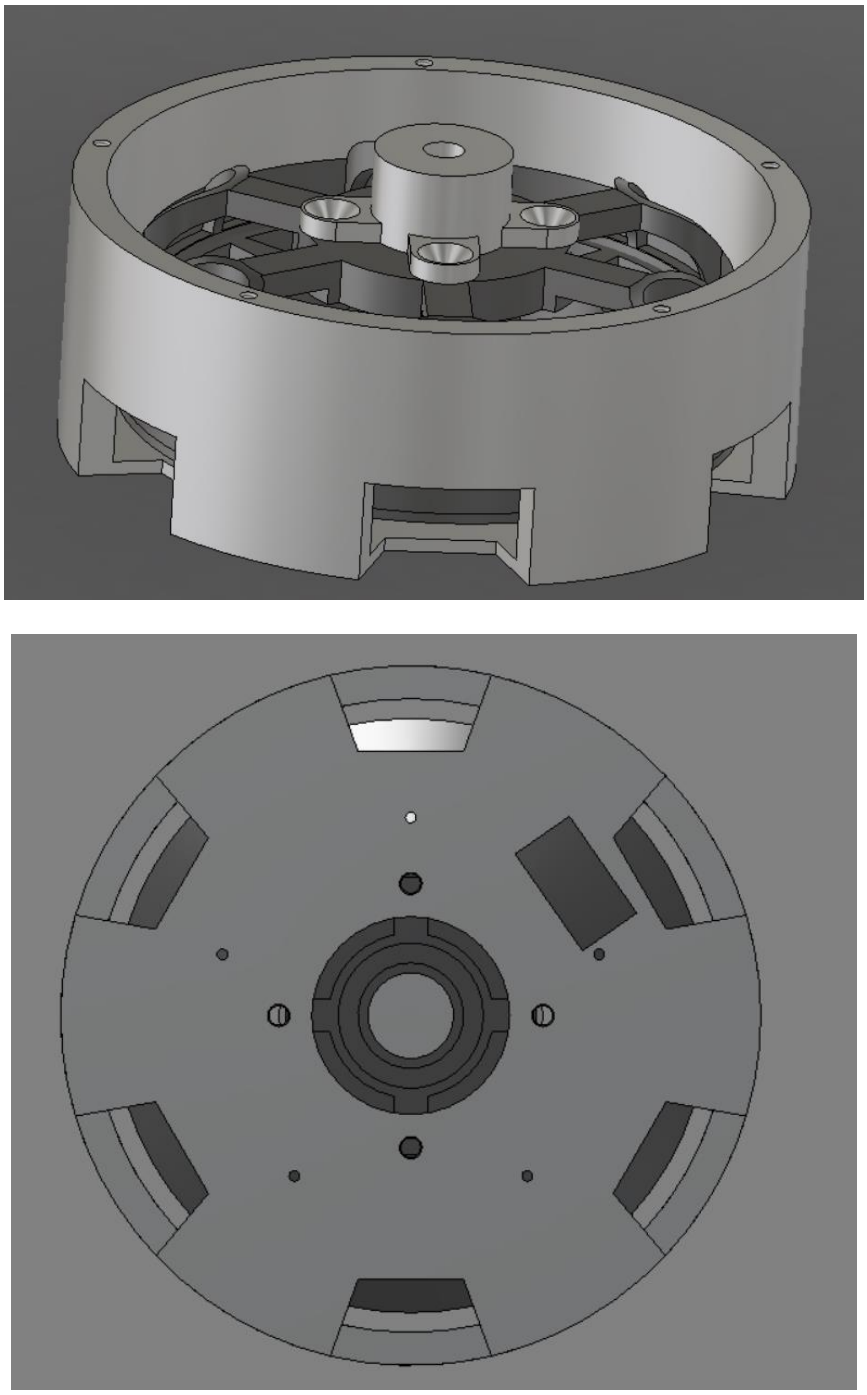

Figure 16: Orthographic and Rear View of Motor Housing

In the Figure you can see that the design has multiple pockets cut in at the bottom of the housing where the motor rotor/stator assembly sits, these are for cooling vents for the motor during high operation. The design and placement of the vents is based on the design of the housing of Ben Katz actuator for the MIT cheetah project. The M4

clearance holes in the structure are aligned with the threaded M4 mounting holes on the back of the motor. These holes also align with the mounting holes on the chosen encoder for this project and allow for the encoder to be mounted directly onto the back of the housing, The large hole in the middle of the housing lets the magnetic encoder get close enough to the spinning magnet on the back of the motor to sense it spinning. The rectangular slot in the upper corner of the rear view is an exit hole for the 3 power/control wires for the brushless motor. The motor housing mounts to the outer flange of the gearbox housing using M3 screws.

3.3 FORCES AND FORCE DISTRIBUTION ON THE CYCLOIDAL DISK

A Cycloidal gearbox is a statically indeterminate system. To obtain forces and stresses on the system a dynamic model should be built using a computer aided approach. Research done by the National Academy of Sciences of Belarus, has helped develop a set of force equations to help model the loads experienced in a cycloidal gearbox during operation. In the operation of a cycloidal gearbox the cycloidal disk remains in contact with half the outer pins in the system at any point during its eccentric rotation. However not all the pins are transmitting a load even though they are still in contact with the disk. The figure below shows the load distribution of an example cycloidal disk. The pins colored in dark blue are loading on the cycloidal disk and the amount shaded corresponds to the percentage of the total loading experienced by the cycloidal disk.

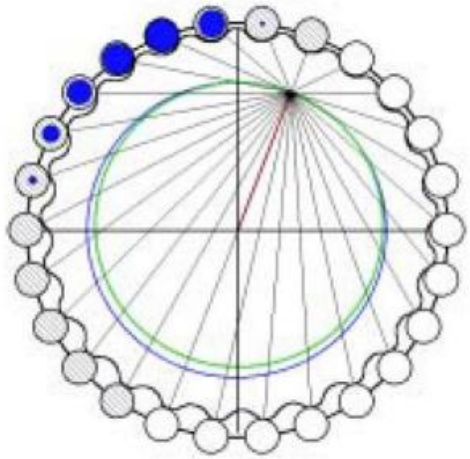

Figure 17: Force Distribution Between Cycloidal Gear and Output Pins *[11]*

In the figure we can see that there are action lines drawn from the tangent point created between the centrode circle of the epicycloid during eccentric motion and the centrode circle for the outer pins which are centered in the gearbox. These action lines give us the contact point of all the engaged pins and allow us to determine the vector of the contact forces between a contacting pin and the cycloidal disk.

Looking at single instance in time for a cycloidal disk we can draw a free body diagram for the 2-D cartesian plane forces acting on the main elements of the disk for a contact point between a pin and the disk. [9].

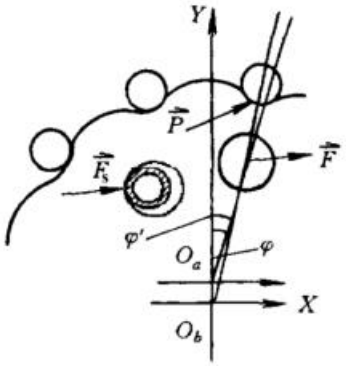

Figure 18: Simplified FBD of a Cycloidal Disk in a Cartesian Plane [12]

In this FBD force P is between the cycloidal disk and the pins. Its value can be calculated using the equation below.

$$P = \sqrt{{P_x}^2 + {P_y}^2}$$

Where P_x can be calculated by:

$$P_x = \frac{Z_4 + M_1}{2K_1 Z_3 r_2}$$

Where Z_4 is the number of pins in the housing, M_1 is the input torque from the input shaft, K_1 is the coefficient of shortening of the epicycloid wheel, Z_3 is the number of convex lobes, and r_2 is the pitch radius of the outer pins [9]. For this design K_1 is set to 1 as it is the ratio of the eccentric radius to the module circle radius. P_y can be calculated by:

$$P_y = \sum_{i=1}^{Z_4/2} \frac{2M_1 \left[\cos\left(\varphi - \frac{2\pi i}{Z_4}\right) - K_1\right] \sin\left(\varphi - \frac{2\pi i}{Z_4}\right)}{K_1 Z_3 r_2 [1 + {K_1}^2 - 2K_1 \cos\left(\varphi - \frac{2\pi i}{Z_4}\right)]}$$

Taking these equations and plugging in the parameters of the designed cycloidal disk the following force plot is shown for the force between the disk and an outer pin as the phi, φ increases and the disk rotates along the pin.

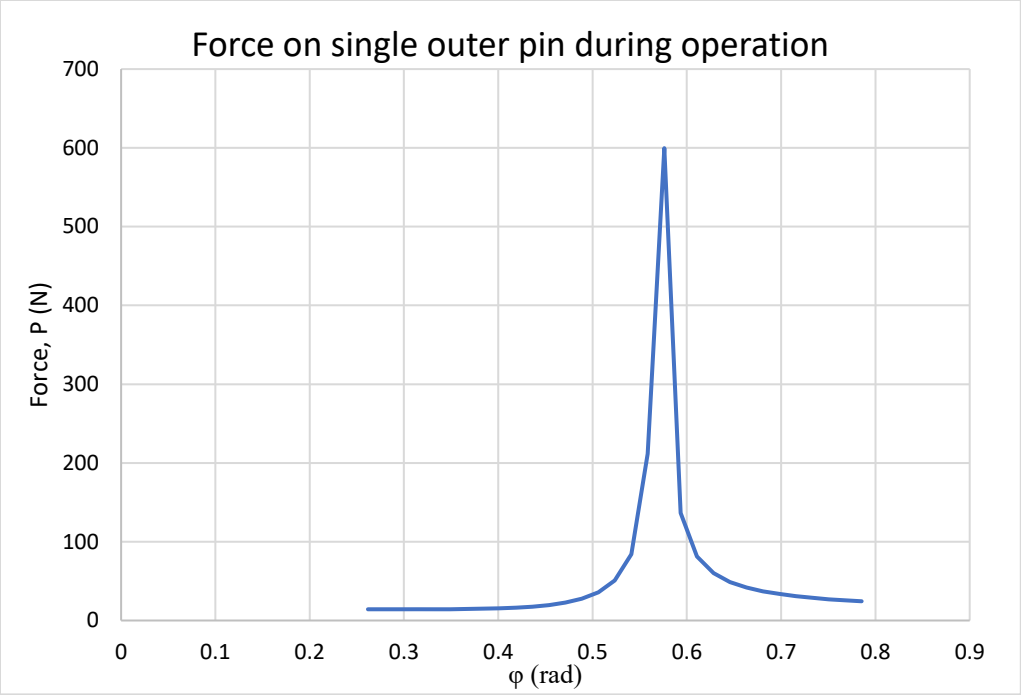

Figure 19: Force on Outer Pin

In the Figure above the force between a single outer pin and the cycloidal disk is plotted for a phi range from the start of a concave lobe to the end. You can see that as the pin slides along the concave pocket the force increases until the pin is just past the middle of the concave region, and then quickly drops off. This makes sense as the max force will be when the next epicycloid lobe on the disk is pushing against the outer pin as the pin rolls out of the pocket.

Referring to the FBD, force $F$is the force between the eccentric spacer and the cycloid disk created from the eccentric pushing the cycloidal disk. This force is flipped in the case of back driving by the output shaft. It can be calculated by:

$$F = \sqrt{{F_x}^2 + {F_y}^2}$$

$$F_x = \frac{1}{n}(P_x + \frac{M_1 \sin(\varphi')}{(Z_1 + Z_2)}$$

$$F_y = \frac{1}{n}(P_y + \frac{M_1 \sin(\varphi')}{m(Z_1 + Z_2)}$$

Where Z_1 and Z_2 represent the number of pins, and the number of concave lobes on the cycloidal disk respectively. The variables n and m represent the number of teeth engaged and the module of the gear. This force is important for bearing selection as the bearing needs to be able to withstand the radial loading but does not affect the disk design or material selection. The calculated force was found to be far below the loads that steel bearings are rated for, and thus was not used as a design factor. F_s represents the force acting between the output shaft rollers and the cycloidal disk. We are only interested in the maximum force exerted on these pins since the pins will be cut from purchased stock material, and thus only the max force, $F_{s\,max}$ needs to be considered for material selection. The equation for calculating $F_{s\,max}$ is:

$$F_{s\,max} = \frac{T_g}{Z_w r_2}$$

Where T_g is the torque per cycloid disc. Z_w is the number of holes in the cycloid disk for output pins and r_2 is the radius of the circle on which the output holes are placed. An assumption is being made that the torque per cycloid disk is evenly distributed [12]. Bending stresses on the pins were not considered in this design as the pins used are very short and made from chromoly steel. The reason chromoly steel was selected was primarily for wear resistance and low friction rather than its material strength as it is significantly stronger than needed. For the designed disk $F_{s\,max}$ was found to be 46.67 N. With the length of the pins being 10mm any bending stress exerted on the pins will be far below 430Mpa σ_y of chromoly steel.

To determine the optimal material to use for the cycloidal disk finite element analysis was performed on the cycloidal disk in 2 separate scenarios to look at stresses in the disk during operation. Femap Student Edition was used for the Finite element analysis work using a NASTRAN solver. Two scenarios were performed on the cycloidal disk. The first scenario simulated a small displacement was applied at the center of the cycloidal disk with the disk constrained in the z axis, and being allowed to rotate about the z, axis. A rigid body element connected to one of the internal edges of the cycloidal disk was modeled to represent an engaged external pin, The load between the pin and the convex lobe was applied based on the equations shown earlier. This was done because in small increments of the cycloidal disk will appear as if it is moving on a tangent line to the eccentric radius. The results of the analysis are shown below.

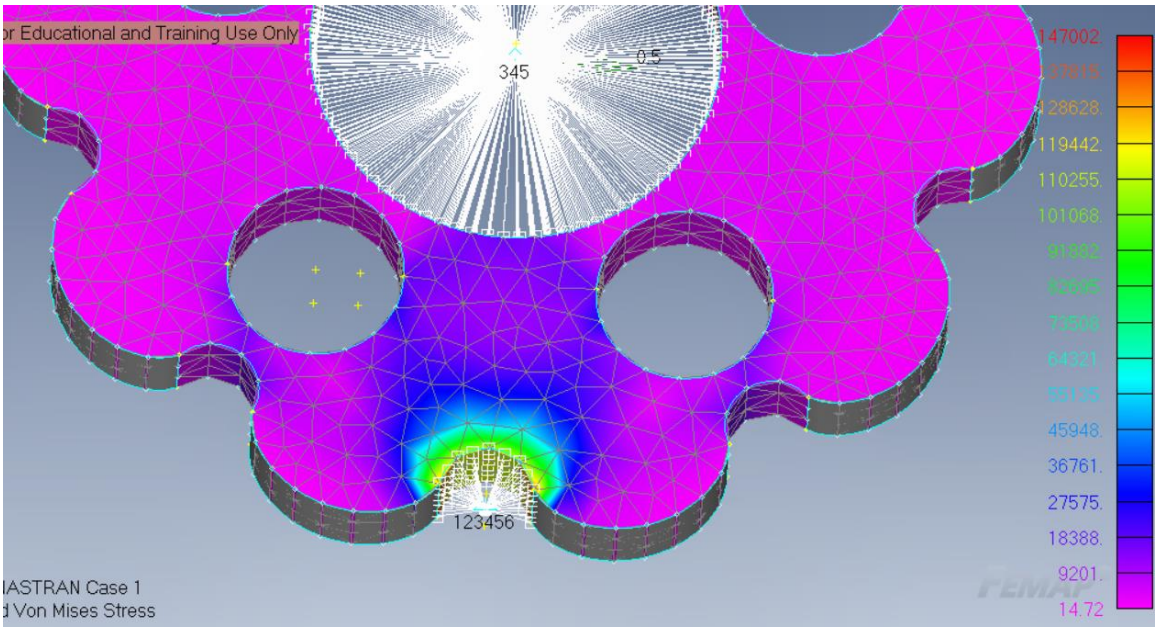

Figure 20: Small Displacement Loading of Cycloidal Disk

In the figure above you can see that the stresses are concentrated around where the cycloidal disk is contacting the external pin. Looking at the output and neglecting singularities in the results the stresses found around the contact point of the external pin read 120Kpa which gives a FOS of 2,000 for Aluminum, and a FOS of 541 for Acetal (Delrin) plastic. This shows initially that we can allow, cost or ease of manufacturing to govern the choice of material in our design rather than strength. This however is not a good representation of the actual system but validates the setup of constraints and loads for a more complex scenario.

The second case simulated was to model the stresses in the disk as it rolls from one pin to the next during operation. First the load applied by the eccentric spacer to the cycloidal disk was applied in the direction perpendicular to the tangent line between the 2 external pins. This force was calculated based on the equations talked about from earlier in this section. This load was applied 3 mm off center from the center of the cycloidal disk to simulate the eccentric loading of the cycloidal disk causing it to rotate around the external pins. Like the last simulation the external pins were represented as rigid body elements contacting the cycloidal disk in its internal edges, with the magnitude of the contact loads between the pin and the disk modeled using the equations earlier in this paper.

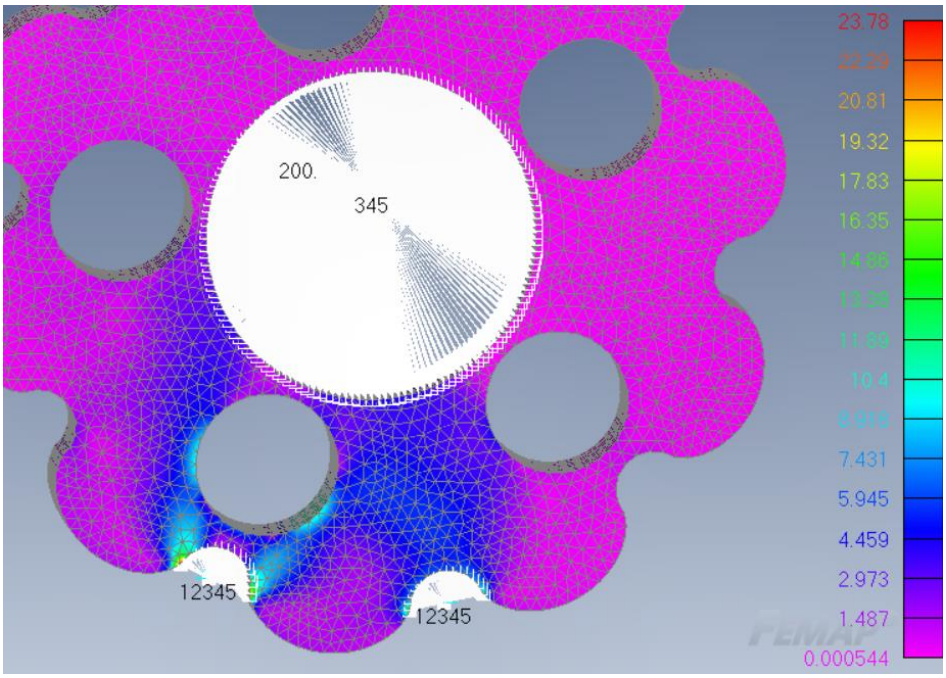

Figure 21: Analysis of Cycloidal Disk at the Point Rolling Between Two Pins

In the analysis the cycloidal disk was modeled to be rotating around the gearbox in a clockwise direction which is why the area at the left pin is experiencing higher stresses due to the disk compressing down on that region. This analysis also shows the stress propagation through the disk when one of the output holes is along the radius to the external pin. Reading the results, the max stresses were found at the right pin having a value of 22.43KPa. This is again significantly lower than the yield stresses of both aluminum and acetal (Delrin) plastic meaning a cycloidal disk made from either material could be used in the cycloidal gearbox. In the secondary prototype to reduce the costs of materials and improve manufacturing lead times the disk was made using FDM additive manufacturing techniques out of polycarbonate. Polycarbonate has a yield strength of 62MPa, which is still much higher than the loads experienced by the disk. Using polycarbonate and 3D printing to create the cycloidal disk allowed for a quicker manufacturing time for components and a further reduction in cost of materials, and not having to rely on out of house manufacturing or paying for CNC time.

3.4 MANUFACTURING

3.4.1 3D PRINTING/ADDITIVE MANUFACTURING

For this project 3D printing was used wherever it could be to help in prototyping and reducing part costs. For this project a high end FDM printer, the Raise3D E2 was sourced from the company Raise 3D. The printer allowed for the ability to print nylon, and Polycarbonate 2 high strength materials that require a hot end that can reach 300 °C. The printer also had a z-height resolution limit of 20 microns, and an X and Y resolution of 0.19 microns; a much finer resolution then many commercially available 3d printers. This allowed for multiple parts of the gearbox prototype and final design to be manufactured.

Figure 22: Raise3D E2 IDEX Printer

Using this printer to print components like the attachment assembly for the electronics, as well as the cycloidal disks helps significantly reduce manufacturing time and cost. By using 3d printing for components it makes the modular actuator easy to produce by a university or individual due to the now widespread access of 3d printers, and the low cost of materials.

3.4.2 OUT OF HOUSE MANUFACTURING

Due to limitations of time and access to the shops during Covid-19 the outer housing of the gearbox was ordered from a CNC shop. Both the prototype and final revisions were manufactured out of 6061-T6 Aluminum. These components cost around $175 each to make, but the final revision has been designed that it could be manufactured in a single operation on any CNC mill. The main reasons for using a part shop for this component were that I did not have the approval in time to use the CNC facilities on campus, and the fast turnaround capabilities of the part shops. This cost was not reflected in the cost sheet as it was considered a development cost.

3.4.3 IN HOUSE MANUFACTURING

The outer pins of the gearbox were turned down from stock ¼ inch White Delrin. To Turn down the right length of material for each pin the material had to stick out a fair amount on the lathe. It was stabilized on the floating end by drilling a center hole and using a live center. For the operation two turning passes were performed with a right to left cutter with a fresh carbide head. The first pass brough the material to within .05” of the spec dimension and then a finer pass was done to reach the 7mm diameter. The reason for this is the Delrin would flex under larger passes which would ruin the concentricity of the pass and bring the part out of tolerance. By making the 2nd pass much finer, the perpendicular force of the cutter against the material is reduced keeping the material from bending while being turned, maintaining concentricity. After the material was turned down each turned down piece was parted into 2 pins for the gearbox. The steel output pins, were also cut to size using a cutoff wheel from chromoly steel stock. All holes in 3D printed parts and metal parts were tapped in the on-campus shops. Assembly of the prototype was also done on campus to show that the gearbox can be manufactured and assembled using tools found in a university metal shop.

3.6 MOTION BOARD AND ENCODER SELECTION

A copy of the motion board developed by Ben Katz from MIT was used for testing and control of the actuator for this thesis. The motion board was purchased from Ali Express for $80. The software being run on the motion board is the firmware written by Ben Katz used for the MIT Cheetah III. The software allows for tracking and zeroing an attached magnetic encoder, as well as implanting torque control when set to motor mode. From initial testing of the firmware it seems to get soft locked when it tries to read the encoder, if there is no encoder attached. Future efforts should be made to develop an in house PCB and firmware, as the features and compatible hardware for this motion board and firmware are very limiting in both usage, and mounting requirements on the actuator.

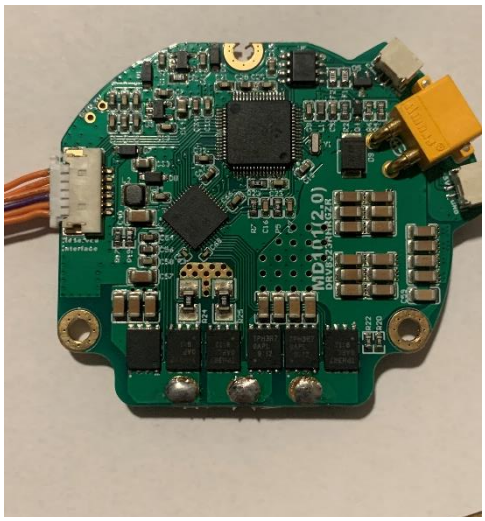

Figure 23: Motion Board used with Custom Encoder Connector Installed

An encoder is needed to track the position of the motor to utilize torque control capabilities of the motion board. The software used on the motion board requires an AS5147 encoder.

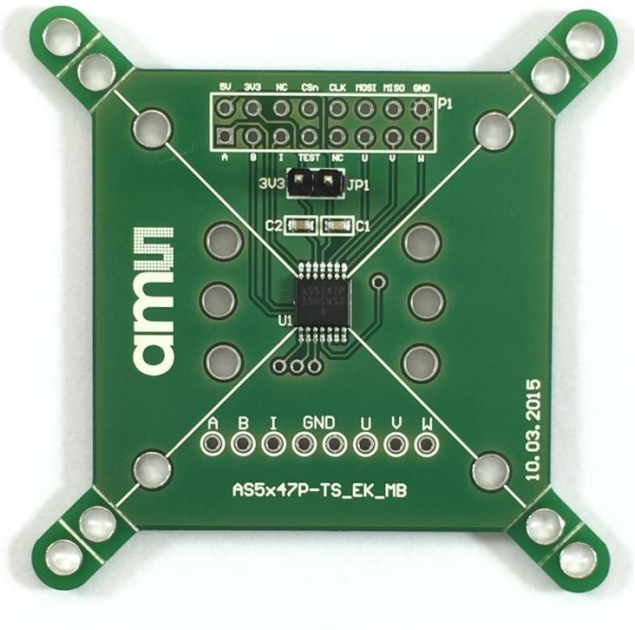

Figure 24: AS5147 Encoder on a Motor Mounting Board

This encoder is a magnetic encoder, designed to be mounted onto the back of a motor. A magnetic encoder works by tracking the change in the magnetic field generated by a magnet to determine the rotational position of the object the magnet is attached to. The magnet must be diametrically polarized so that as it rotates the encoder can detect a polarity change.

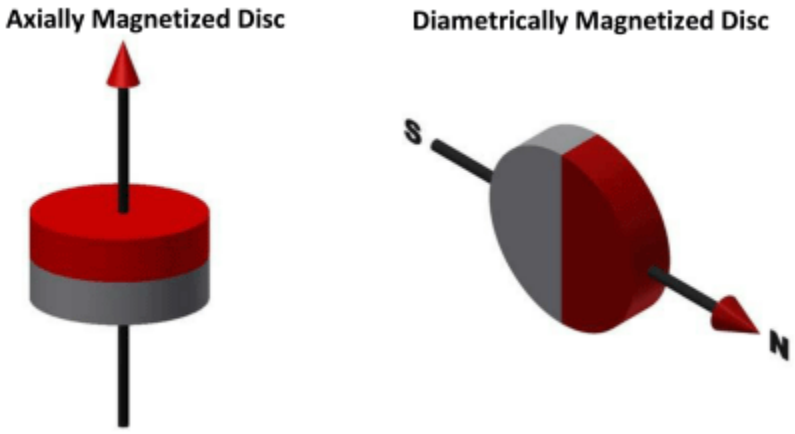

Figure 25: Difference Between an Axially and Diametrically Polarized Magnet

An 8mm x 3mm magnet was chosen for this task based on the recommendations from the datasheet for the AS5147 encoder. The magnet is mounted in the back portion of the hollow through shaft of the motor as, the ID of the shaft is 8mm. The encoder board screws onto the back of the actuator motor housing using the same screws that mount the motor to the motor housing.

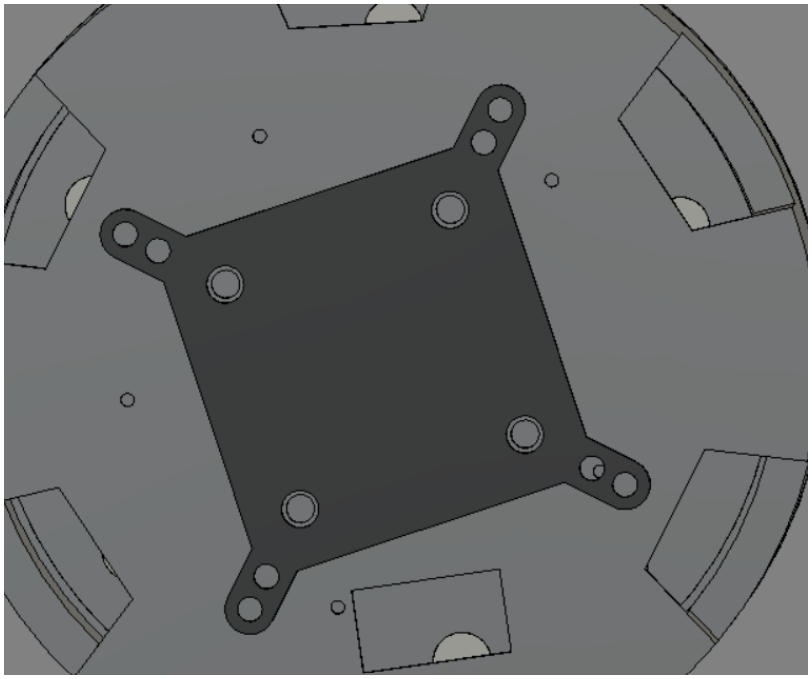

Figure 26: CAD Model of Encoder Mounted to back of Motor Sheath

This creates a very simple mating interface for the encoder to the actuator and will make it easy in the future if the encoder ever needs to be swapped out. It also protects the surface mount components on the PCB as they sit slightly inset of the actuator housing, rather than being exposed. To connect the encoder to the motion board a special connector needed to be created to plug into the motion board. The motion board required use of a MOLEX PanelMate 51146 6 pin connector with a 1mm pitch. To create the custom connector a micro crimper was acquired to properly crimp the 1mm pitch Molex connectors. 26 awg wire was used for the cable as specified by the crimp connectors datasheet. The wires were then spliced to 1.4mm pitch breadboard jumper

cables so that the encoder side of the connector could interface with the encoder dev board.

Having to make this connector was a large drawback of the motion board used for this project. The 1mm pitch connectors require a specialized crimping tool that is much more expensive than a standard pitch range crimper. For future work with this project, it is recommended that a custom PCB be designed using larger pitch connectors to make for easier assembly. This would also remove the cost of purchasing a micro pitch crimper for fabrication.

3.7 TESTING

With the first gearbox prototype completed, 2 tests were performed to evaluate the design. The first test was to test the actuators' ability to create the 7Nm output torque required from the initial project requirements. The other test performed was a long-term operation test. The reason for this test is it is difficult to approximate the wear life of the cycloidal disks in the gearbox, due to the standard endurance life calculations using gears. Since the cycloidal disks are shaped different than gears it seemed necessary to perform a long-term operation test to evaluate the wear life of these components. To do this the actuator system was powered by a brushless ESC and the output speed was set to 60 rpm. This was done by tracking a marked line on the gearbox and measuring the amount of time required for one full revolution of the output disk. This meant that the

cycloidal disks would complete 36,000 revolutions per hour; completing 864,000 revolutions over a 24 hour period. During the initial test with the first prototype failure occurred at the 6-hour mark with the motor shaft adaptor. The input shaft sat in the adaptor as an interference fit, but over long-term operation had rubbed away to a clearance fit such that the motor was no longer spinning the input shaft. To fix this a flat was ground into the input shaft and the motor adaptor part was modified to include a tapped M3x0.5 hole for a set screw to be used to lock the input shaft in place. The test was then rerun with the new motor adaptor installed. With the new adaptor installed the gearbox operated without failure for 24 hours. Post run the gearbox was disassembled and inspected a picture of some components are below.

Figure 27: Wear Marks on Gearbox Case from Endurance Testing

From the Figure you can see that there was some material wear inside the gearbox housing from rubbing of the cycloidal disk against the outer pins. While the wear was low it is important to try and reduce this so a silicon grease was dressed along the cycloidal profile to further reduce friction between the 2 surfaces. Additionally, a thin 0.6mm nylon washer was placed between the bottom cycloidal disk and the bottom of the gearbox housing to add clearance between the 2. With this change the test was performed again

with a new gearbox housing and the gearbox was run for 30 hours. This meant the cycloidal disks completed 1,080,000 revolutions which it completed without failure. This was deemed to be sufficient proof that the gearbox would survive continuous operation in a robotic assembly.

The gearbox was then subjected to a torque test using the motion board/ encoder assembly. For this test a testing arm was developed that would carry 2kg of mass centered at the end of the arm. The mass of the test arm was neglected. The weight was added to the arm using lead weights.

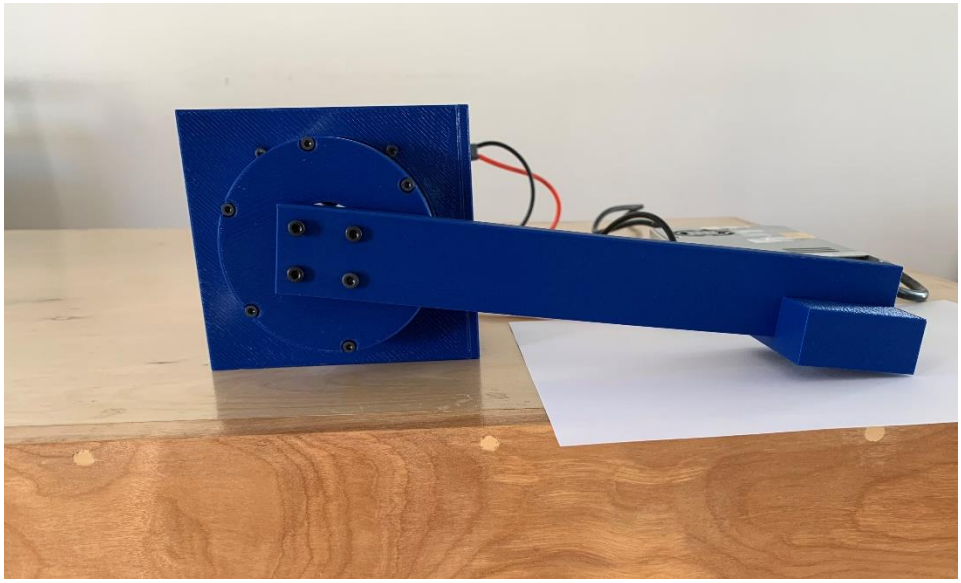

Figure 28: Torque Testing Setup with Arm Mounted

Using the firmware connected to the motion board with the encoder calibrated and the operation set to motoring. 1 N/m of torque was set as the input torque into the gearbox and was to be held. The arm was then observed to see if the gearbox was able to develop the 7 N/m of torque required to overcome the mass of the arm and move it off the table. The time it took to move the mass was also recorded, as an important aspect

of the actuator is the instantaneous delivery of torque. The average reaction time for motor movements for humans is 273ms, so this was the standard used as comparison to determine if the torque was being delivered fast enough. The tests were each recorded using a camera and were played back to determine the exact timing.

Table 5: Results on Time Response for Torque Testing

Trial	Response Time
1	0.21
2	0.21
3	0.17
4	0.21
5	0.20

The test was successful, and the gearbox was able to deliver the torque required to move the arm. In the table above it can be seen that the average response time for the response from the arm was measured to be 200ms. While this is faster than the average measured human response time, it would be preferrable to minimize this for better response control in the robot. This delay could be attributed to firmware or hardware. The delay in hardware comes in the form of backlash in the system. The measured backlash in the gearbox system with new components was measured to be .02mm. This

is very low for a gearbox system and so it is likely that some of this delay is coming from firmware response times, and error in measurement during the test. These tests were performed in ambient temperature conditions. There was no testing done at elevated temperature to simulate performance of the actuator when significant joule heating occurs. Polycarbonate filament has a thermal resistance to 140 °C, which should exceed the temperature of the actuator under operating conditions.

4.0 CONCLUSION

The objective of this thesis was to develop a proprioceptive actuator utilizing a cycloidal gearbox that can meet the operating conditions for the Cal Poly Legged Robotics projects and act as a comparison to off the shelf actuators that are currently commercially available. The cycloidal gearbox proved to be reliable and able to handle the high torque demands required by the gearbox. Further it shows that a cycloidal gearbox can be manufactured using cheaper manufacturing methods, like additive manufacturing, compared to gears used in traditional planetary gearboxes. This allows for manufacturing of the gearbox, or modifications to the current design to be carried out in a university at a significantly lower cost. While the design was not able to be packaged into a similar envelope as the T80 actuators currently being used, I believe that the current design can be further optimized to reduce package size.

4.1 FURTHER RESEARCH AND RECOMMENDATIONS

After reviewing the project, I would like to recommend areas where I believe work can be done further to improve the design and packaging of the actuator. An analysis of vibration in the gearbox should be done to see if a single disk gearbox is feasible. Much of the gearbox’s weight comes from the metal housing for the cycloidal pins and disk. Because of this the rotating cycloidal disks change the c.o.m during operation less than

originally expected. I believe a vibration analysis would show that only one disk may be necessary rather than a 2nd disk to cancel out the off-center mass rotation of the disks. The project would benefit from the design of a custom motion board for the actuators. The off the shelf motion boards currently being used, utilize out of date connectors, and lack good documentation on the firmware and hardware mounted on the board. Because of this there was a lot of time spent troubleshooting the operation of the motion board and making custom connectors for the motion board utilizing specialized crimping tools. The project would benefit from a torque testing setup that allowed for better testing of instantaneous torque control rather than relying on a mass-based setup and timing. Using a system that utilizes an eddy current brake, and a torque sensor would be useful for testing future actuator designs.

Further work needs to be done on the actuator design to improve the joining the motor and gearbox in the actuator assembly if a cycloidal gearbox is to be used. Unlike current designs that integrate the planetary ring gear inline to the motor rotor, the cycloidal gearbox cannot be driven by the outer pins. Further work in motor selection is needed to find a smaller package. Additionally, I believe that the gearbox reduction ratio could be easily increased allowing for a smaller lower power motor to be used. Further research could be done into a motor that is centerless but allows for the mounting of a back adaptor to drive a floating input shaft to use the current gearbox design.

REFERENCES

[1] B. Kwan, "Modeling and Control of a Vertical Hopping Robot," Califronia Polytechnic University, San Luis Obispo, 2021.

[2] P. M. Wensing1, A. Wang, S. Sangok, D. Otten, J. Lang and S. Kim, "Proprioceptive Actuator Design in the MIT Cheetah: Impact Mitigation and High-Bandwidth," MIT, Massachusetts, 2016.

[3] T. H. Massie and J. K. Salisbury, "The PHANToM Haptic Interface:," *ASME Dynamic Systems and Control,* vol. 1, no. 55, 1994.

[4] R. M. Walter and D. R. Carrier, "Ground Forces applied by Galloping Dogs," *The Journal of Experimental Biology,* no. 210, pp. 208-216, 2007.

[5] S. Sang, M. Chuah, J. Yee and H. Dong, "Design Principles for Energy-Efficient Legged Locomotion and Implementation on the MIT Cheetah Robot," *IEEE/ASME Transactions on Mechatronics,* vol. 3, no. 20, pp. 1117-1129, 2015.

[6] B. Katz, "Low Cost, High Performance Actuators for Dynamic," Massachusetts Institute of Technology , Cambridge, 2016.

[7] B. Katz, "A low cost modular actuator for dynamic robots," Massachusetts Institute of Technology, Cambridge, 2018.

[8] W.-S. Lin, "Design of a two-stage cycloidal gear reducer with tooth modifications," *Mechanism and Machine Theory,* vol. 79, pp. 184-197, 2014.

[9] H. Hansson, "Design of a Planetary-Cyclo-Drive Speed Reducer Cycloid Stage," 30 05 2012. [Online]. Available: http://edge.rit.edu/edge/P16201/public/P15201%20files/Research%20Papers%20Humanoids/2012%20-%20Design%20of%20a%20Planetary-Cyclo-Drive%20Speed%20Reducer%20Cycloid%20Stage%20%2C%20Geometry%20%2C%20Element%20Analyses%20-%20Borisov%2C%20Panchev.pdf. [Accessed 25 8 2021].

[10] O. Alipiev, "Geometry and Forming of Epi- and Hypo-Cycloidal Toothed Wheels in

Modified Cyclo-Transmission," *Ph.D. Dissertation, Ruse,* pp. 1-36, 1988.

[11] D. Tsetserukou and V. Bansinuk, "Contact Force Distribution Among Pins of Trochoid Transmissions," Department of vibroprotection of machines, Institute of Mechanics and Reliability of Machines of the NAS Belarus, Minsk, 2012.

[12] W. Yao and Z. Zhang, "Dynamic Load Analysis of the Bearing of the Revolving Arm of the RV Transmission Mechanism," *Journal Of Beijing, Institute of Machinery Industry,* pp. 5-8, 1997.

APPENDICES

A: DRAWINGS AND BOM

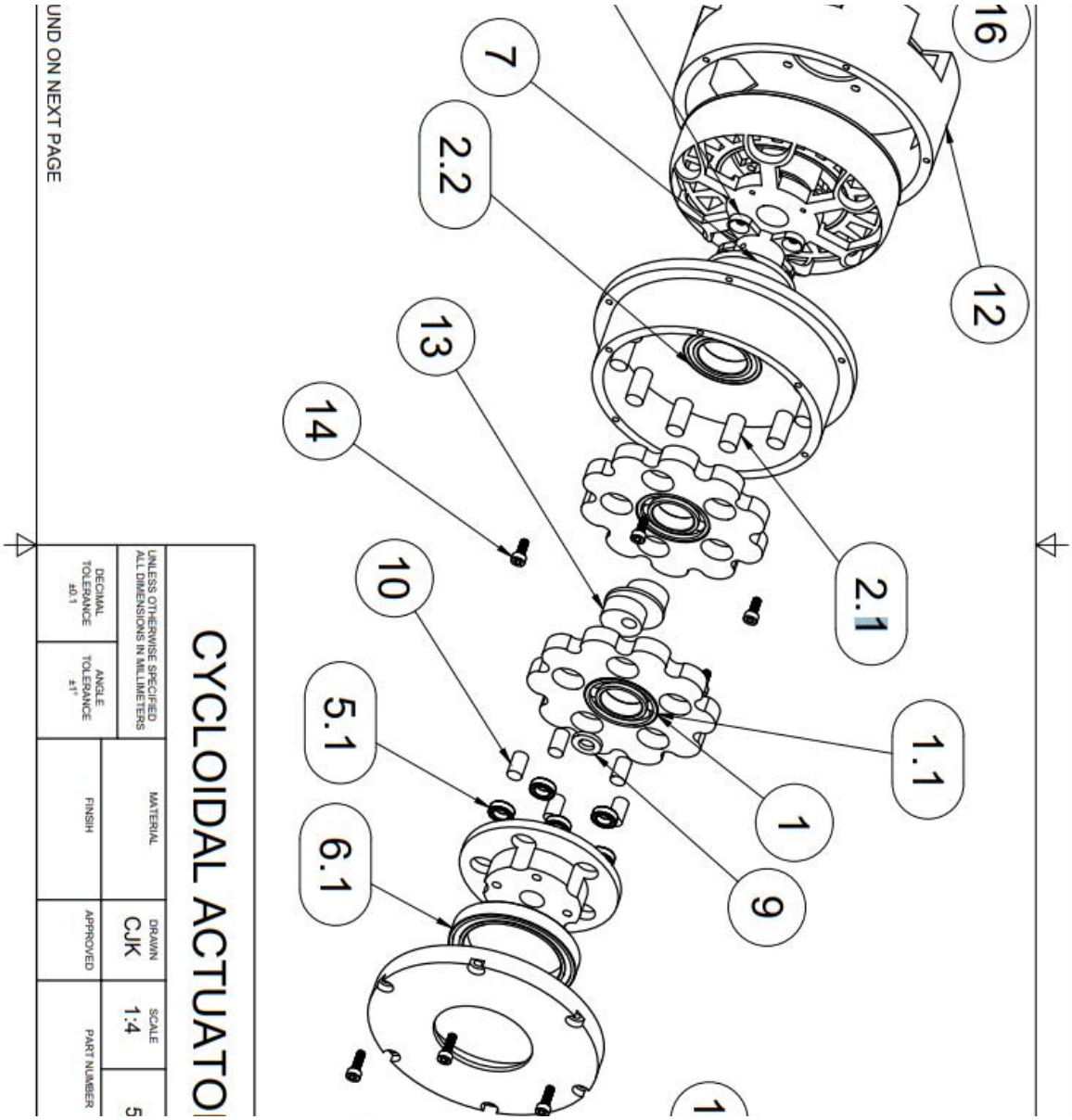

PARTS LIST			
ITEM	QTY	PART NUMBER	MATERIAL
1	2	10:1 7MM CYCLOID DISK	
1.1	1	6656K98_ULTRA-THIN BALL BEARING	STEEL
2	1	CYCLOID FRAME	
2.1	11	7MM CYCLOID PIN	ACETAL RESIN, WHITE
2.2	1	5972K279_BALL BEARING	STEEL
3	1	MOTOR MOUNT	ALUMINUM 6061
5	1	OUTPUT DISK	
5.1	6	7487N55_PRECISION STAINLESS STEEL BALL BEARING	STEEL
6	1	GEARBOX TOP_COVER	
6.1	1	6656K221_ULTRA-THIN BALL BEARING	STEEL
7	1	95610A460_NYLON PLASTIC WASHER	NYLON 6
8	1	6MM DRIVE SHAFT	STEEL
9	2	91545A450_LUBRICANT-FILLED NYLON PLASTIC WASHER	NYLON 6
10	5	6MM TRANSLATION SHAFT	STEEL
11	1	EAGLEPOWER 8308 MOTOR	STEEL
12	1	MOTOR SHEATH	PLASTIC, OPAQUE WHITE
13	1	JOINT ECCENTRIC SHAFT	PLASTIC, OPAQUE WHITE
14	5	91274A103_M3X0.5 8MM SOCKET HEAD SCREW	STEEL
15	6	91274A105_M3X0.5 10MM SOCKET HEAD SCREW	STEEL
16	1	AMS5X47_MOTORBOARD_LAYOUT	FR4

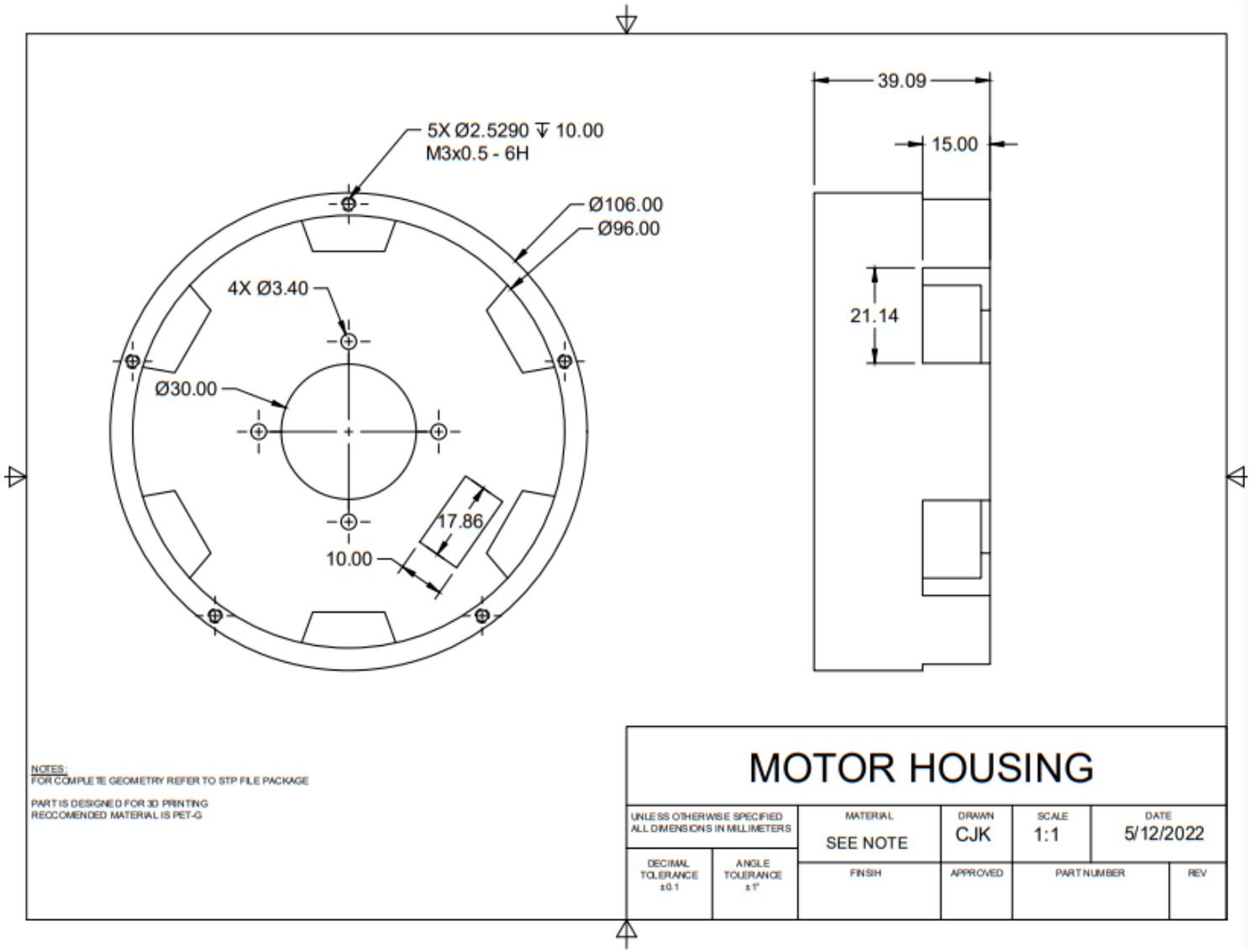
5X Ø2.5290 ↧ 10.00
M3x0.5 - 6H
Ø106.00
Ø96.00
4X Ø3.40
Ø30.00
17.86
10.00
39.09
15.00
21.14
NOTES:
FOR COMPLETE GEOMETRY REFER TO STP FILE PACKAGE
PART IS DESIGNED FOR 3D PRINTING
RECCOMENDED MATERIAL IS PET-G
MOTOR HOUSING
UNLESS OTHERWISE SPECIFIED
ALL DIMENSIONS IN MILLIMETERS
MATERIAL
SEE NOTE
DRAWN
CJK
SCALE
1:1
DATE
5/12/2022
DECIMAL TOLERANCE
±0.1
ANGLE TOLERANCE
±1°
FINISH
APPROVED
PART NUMBER
REV

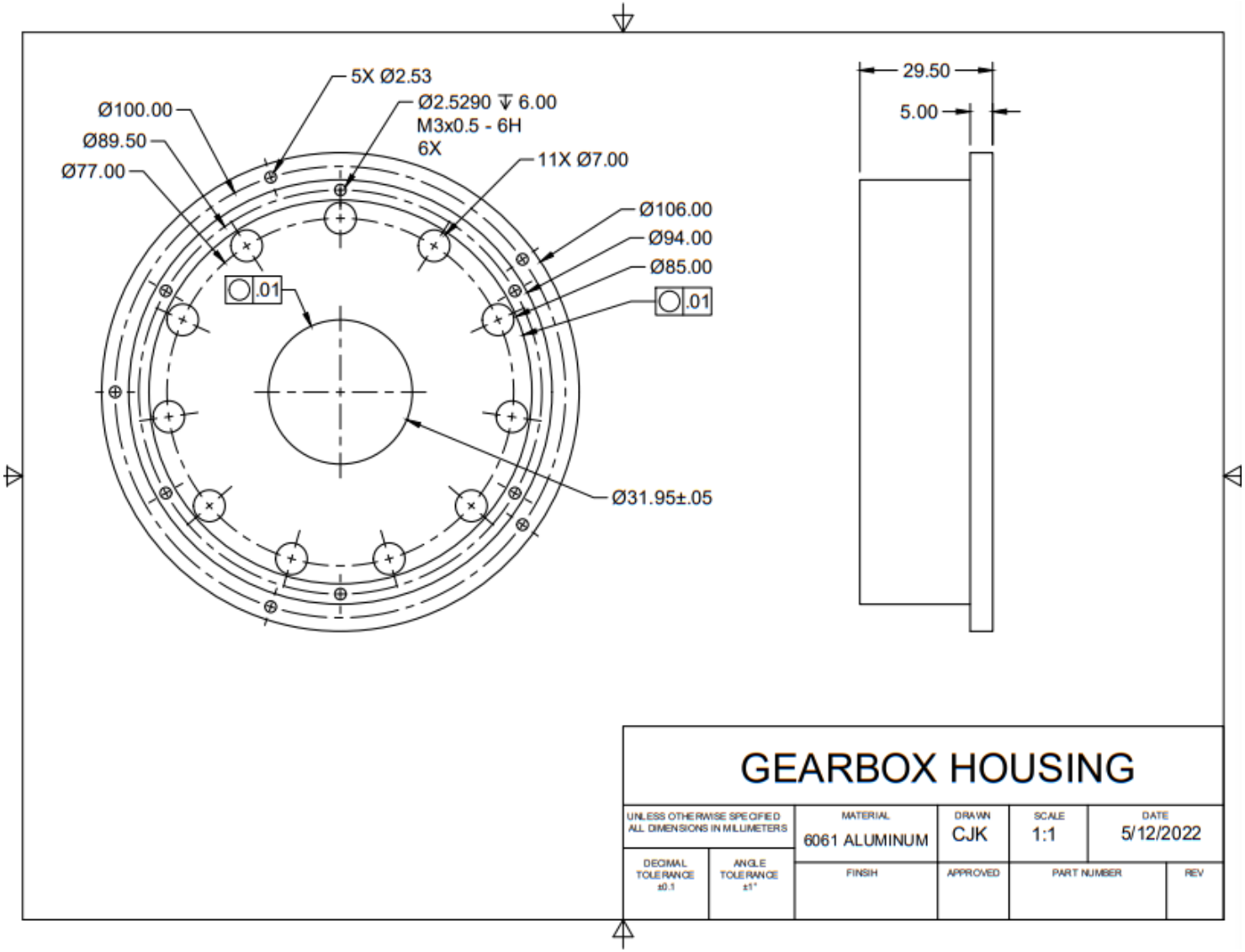
5X Ø2.53
Ø2.5290 ↧ 6.00
M3x0.5 - 6H
6X
Ø100.00
Ø89.50
Ø77.00
11X Ø7.00
Ø106.00
Ø94.00
Ø85.00
.01
.01
Ø31.95±.05
29.50
5.00
GEARBOX HOUSING
UNLESS OTHERWISE SPECIFIED
ALL DIMENSIONS IN MILLIMETERS
MATERIAL
6061 ALUMINUM
DRAWN
CJK
SCALE
1:1
DATE
5/12/2022
DECIMAL TOLERANCE
±0.1
ANGLE TOLERANCE
±1°
FINISH
APPROVED
PART NUMBER
REV

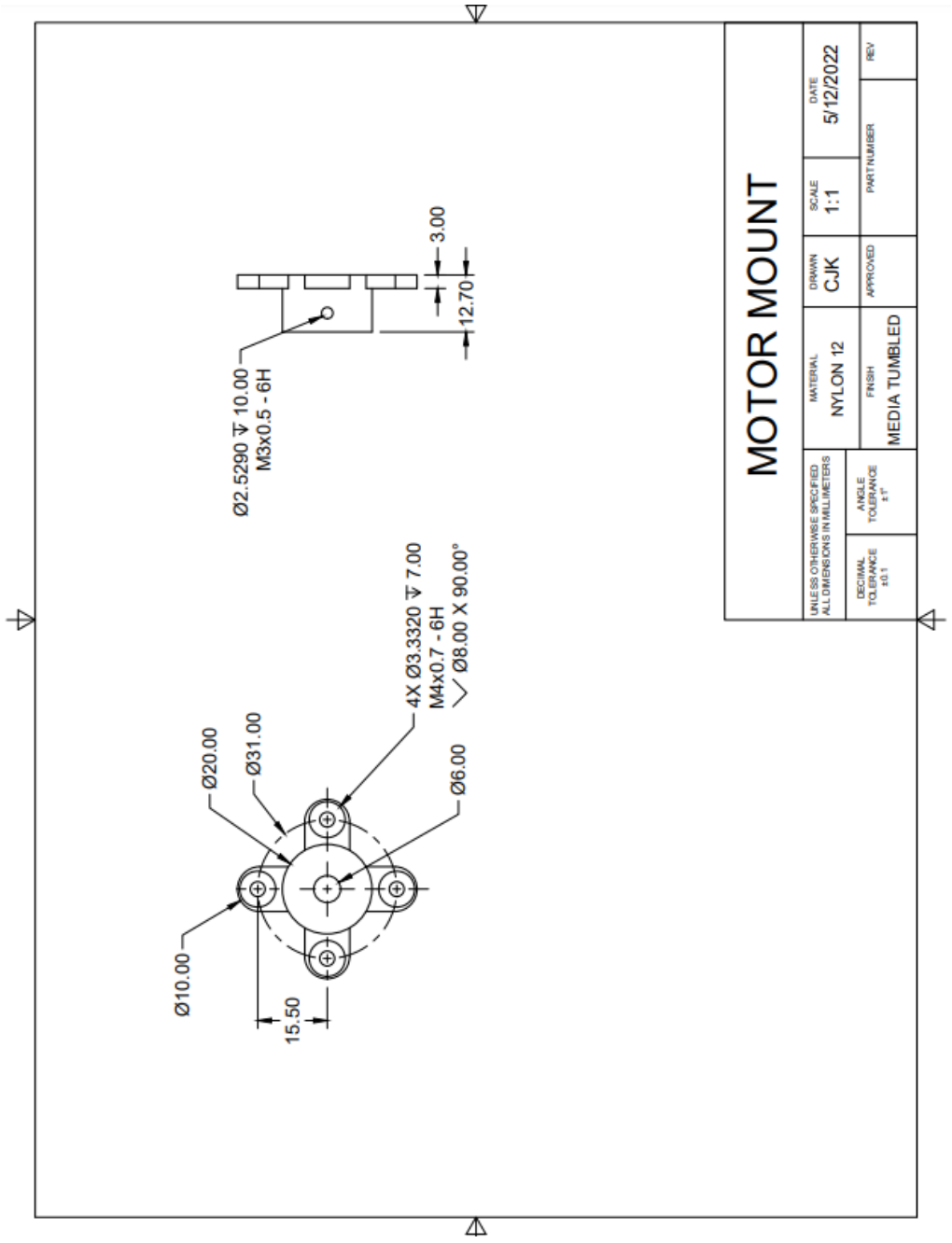
MOTOR MOUNT
UNLESS OTHERWISE SPECIFIED ALL DIMENSIONS IN MILLIMETERS
DECIMAL TOLERANCE ±0.1
ANGLE TOLERANCE ±1°
MATERIAL NYLON 12
FINISH MEDIA TUMBLED
DRAWN CJK
APPROVED
SCALE 1:1
PART NUMBER
DATE 5/12/2022
REV
3.00
12.70
Ø2.5290 ↧ 10.00
M3x0.5 - 6H
4X Ø3.3320 ↧ 7.00
M4x0.7 - 6H
⌵ Ø8.00 X 90.00°
Ø20.00
Ø31.00
Ø6.00
Ø10.00
15.50

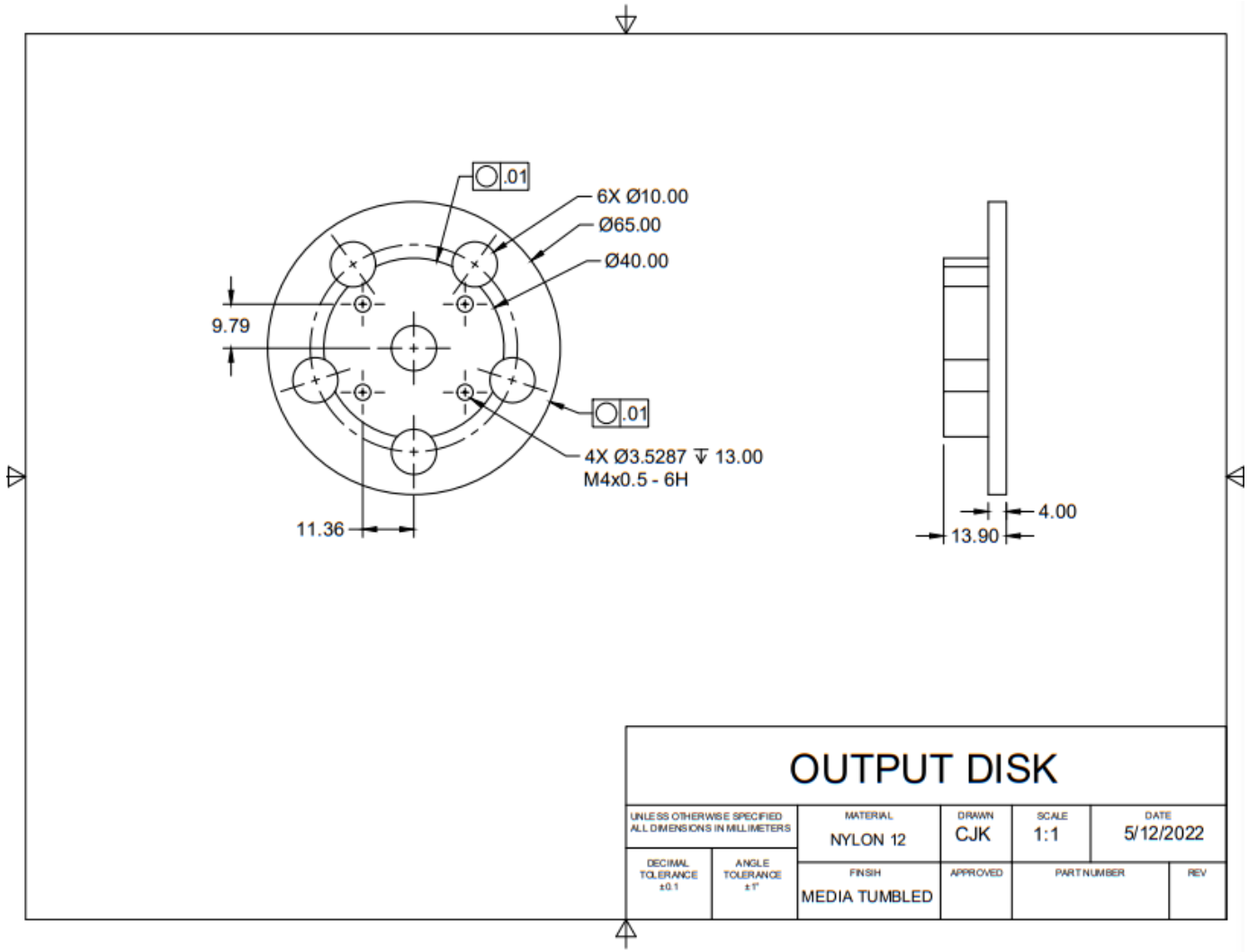
.01
6X Ø10.00
Ø65.00
Ø40.00
9.79
.01
4X Ø3.5287 ↧ 13.00
M4x0.5 - 6H
11.36
4.00
13.90
OUTPUT DISK
UNLESS OTHERWISE SPECIFIED
ALL DIMENSIONS IN MILLIMETERS
MATERIAL
NYLON 12
DRAWN
CJK
SCALE
1:1
DATE
5/12/2022
DECIMAL TOLERANCE ±0.1
ANGLE TOLERANCE ±1°
FINISH
MEDIA TUMBLED
APPROVED
PART NUMBER
REV

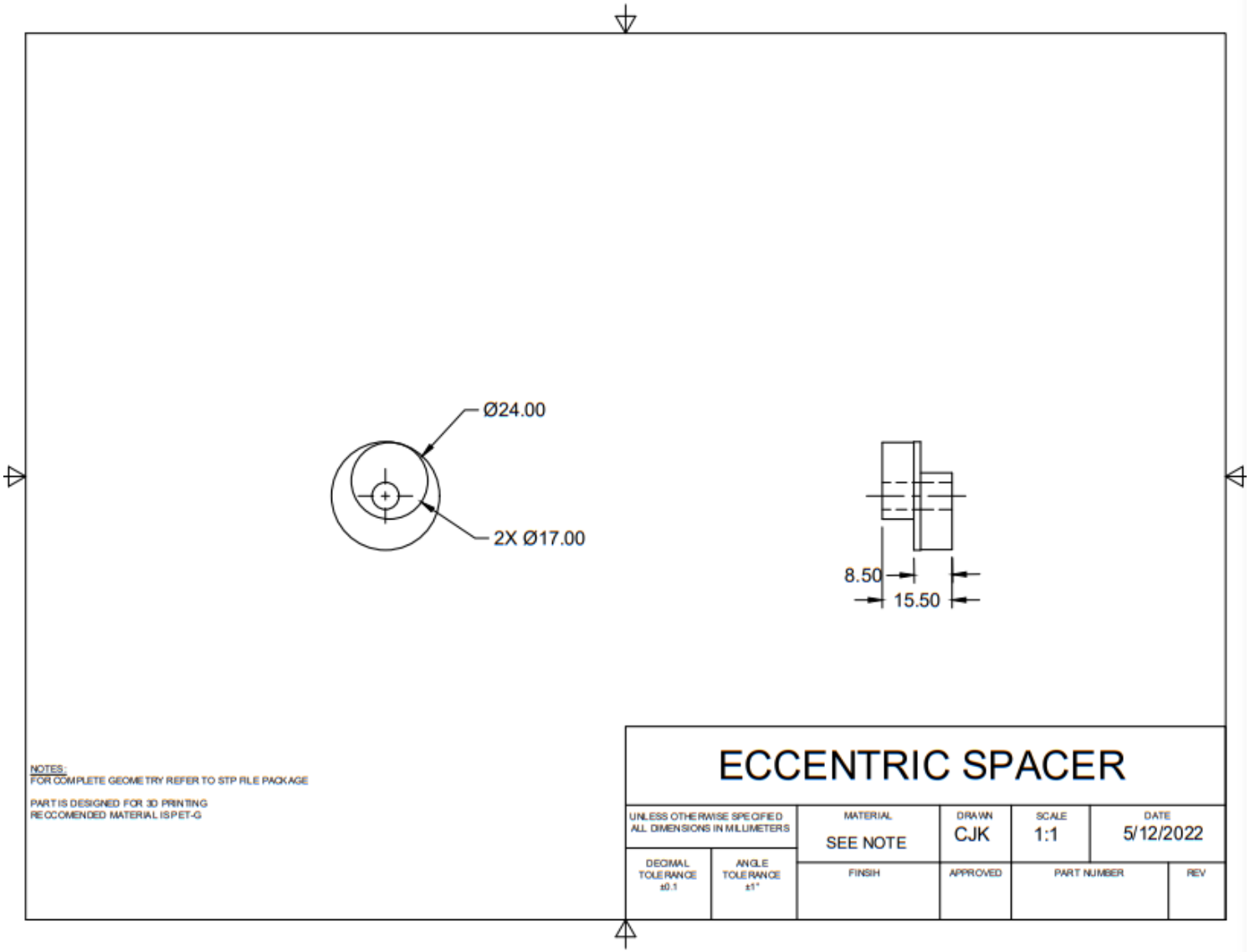
Ø24.00
2X Ø17.00
8.50
15.50
NOTES:
FOR COMPLETE GEOMETRY REFER TO STP FILE PACKAGE
PART IS DESIGNED FOR 3D PRINTING
RECCOMENDED MATERIAL IS PET-G
ECCENTRIC SPACER
UNLESS OTHERWISE SPECIFIED
ALL DIMENSIONS IN MILLIMETERS
MATERIAL
SEE NOTE
DRAWN
CJK
SCALE
1:1
DATE
5/12/2022
DECIMAL TOLERANCE
±0.1
ANGLE TOLERANCE
±1°
FINISH
APPROVED
PART NUMBER
REV

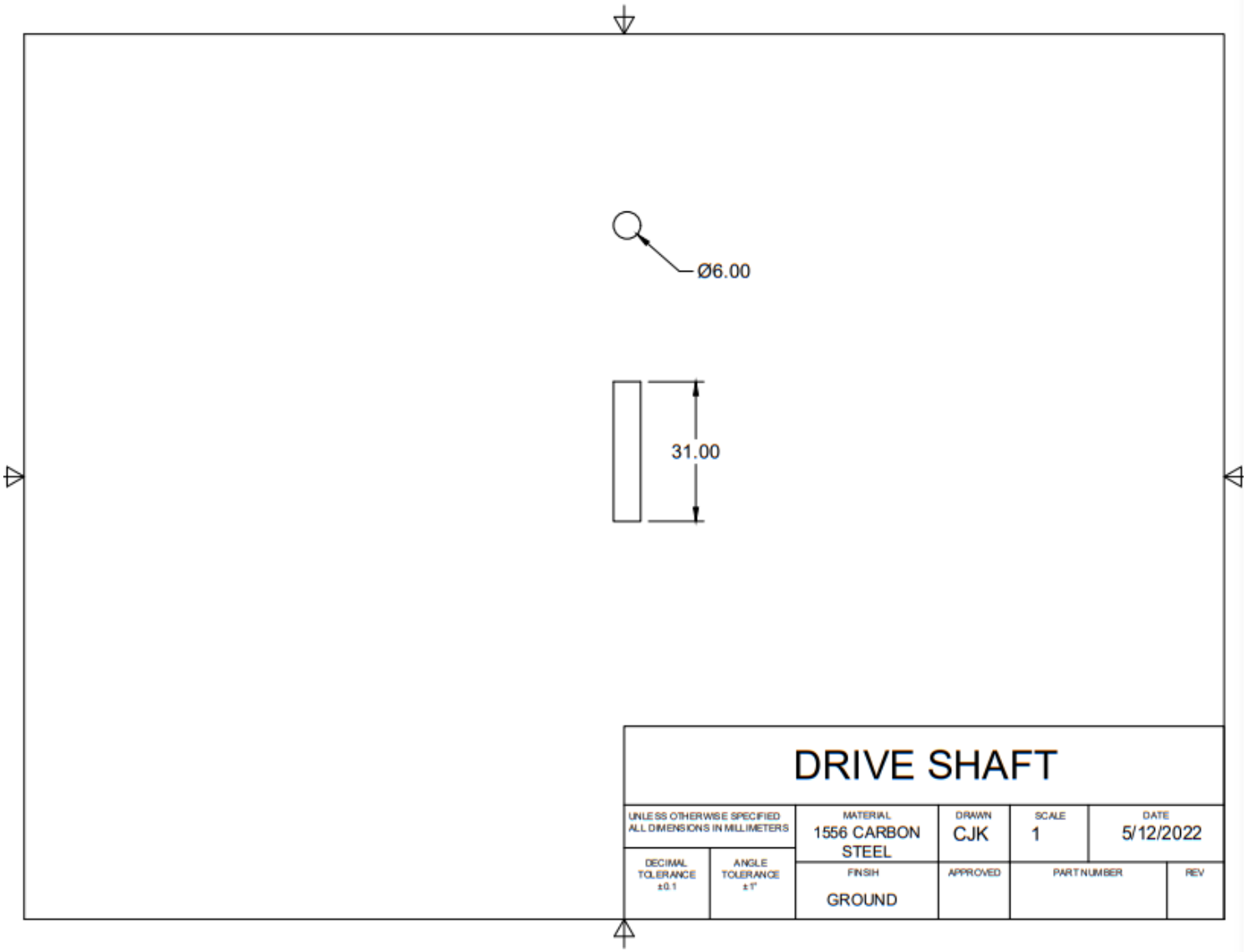
Ø6.00
31.00
DRIVE SHAFT
UNLESS OTHERWISE SPECIFIED ALL DIMENSIONS IN MILLIMETERS
DECIMAL TOLERANCE ±0.1
ANGLE TOLERANCE ±1°
MATERIAL 1556 CARBON STEEL
DRAWN CJK
SCALE 1
DATE 5/12/2022
FINISH GROUND
APPROVED
PART NUMBER
REV

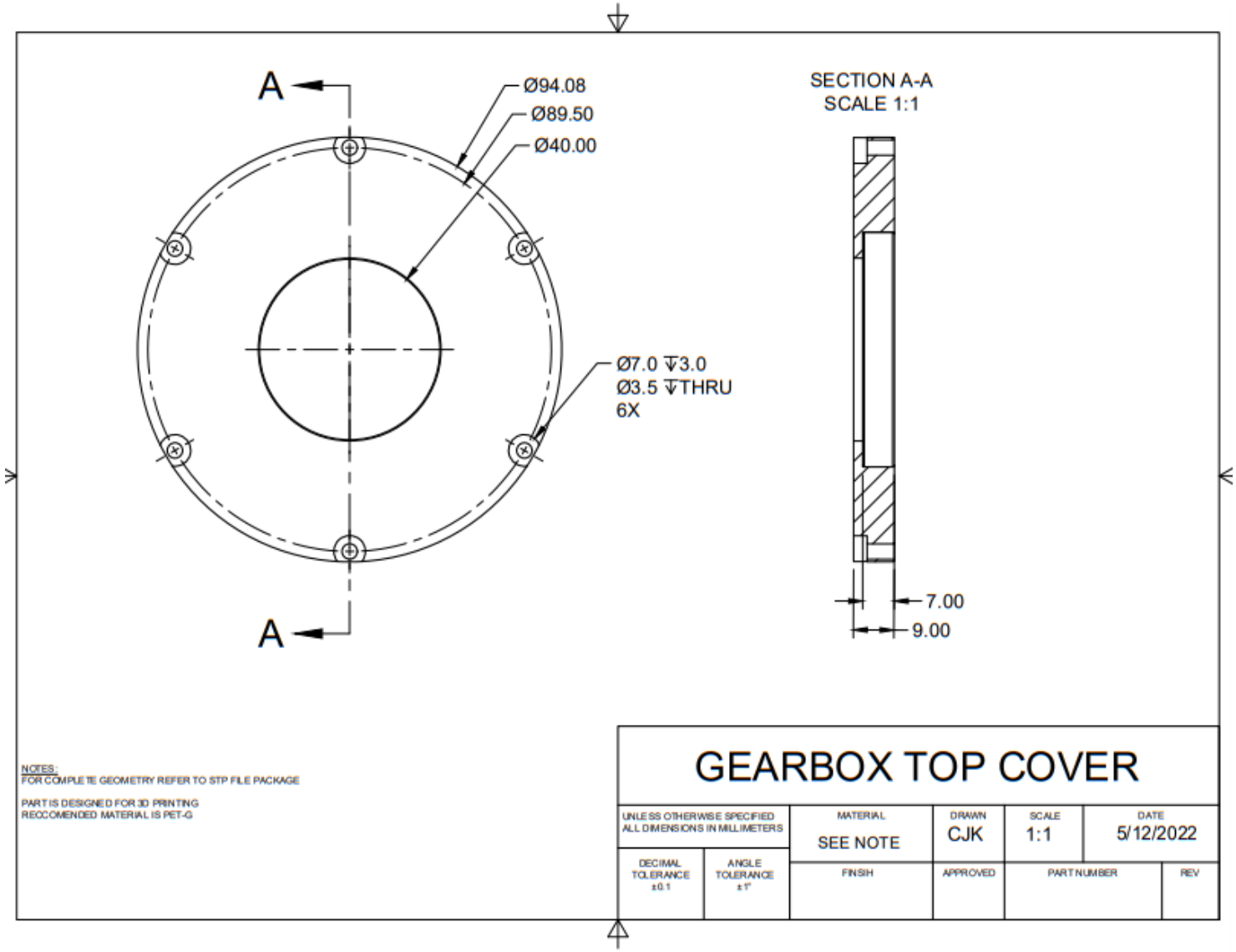
A
Ø94.08
Ø89.50
Ø40.00
Ø7.0 ↧3.0
Ø3.5 ↧THRU
6X
A
SECTION A-A
SCALE 1:1
7.00
9.00
NOTES:
FOR COMPLETE GEOMETRY REFER TO STP FILE PACKAGE
PART IS DESIGNED FOR 3D PRINTING
RECCOMENDED MATERIAL IS PET-G
GEARBOX TOP COVER
UNLESS OTHERWISE SPECIFIED
ALL DIMENSIONS IN MILLIMETERS
MATERIAL
SEE NOTE
DRAWN
CJK
SCALE
1:1
DATE
5/12/2022
DECIMAL TOLERANCE
±0.1
ANGLE TOLERANCE
±1°
FINISH
APPROVED
PART NUMBER
REV

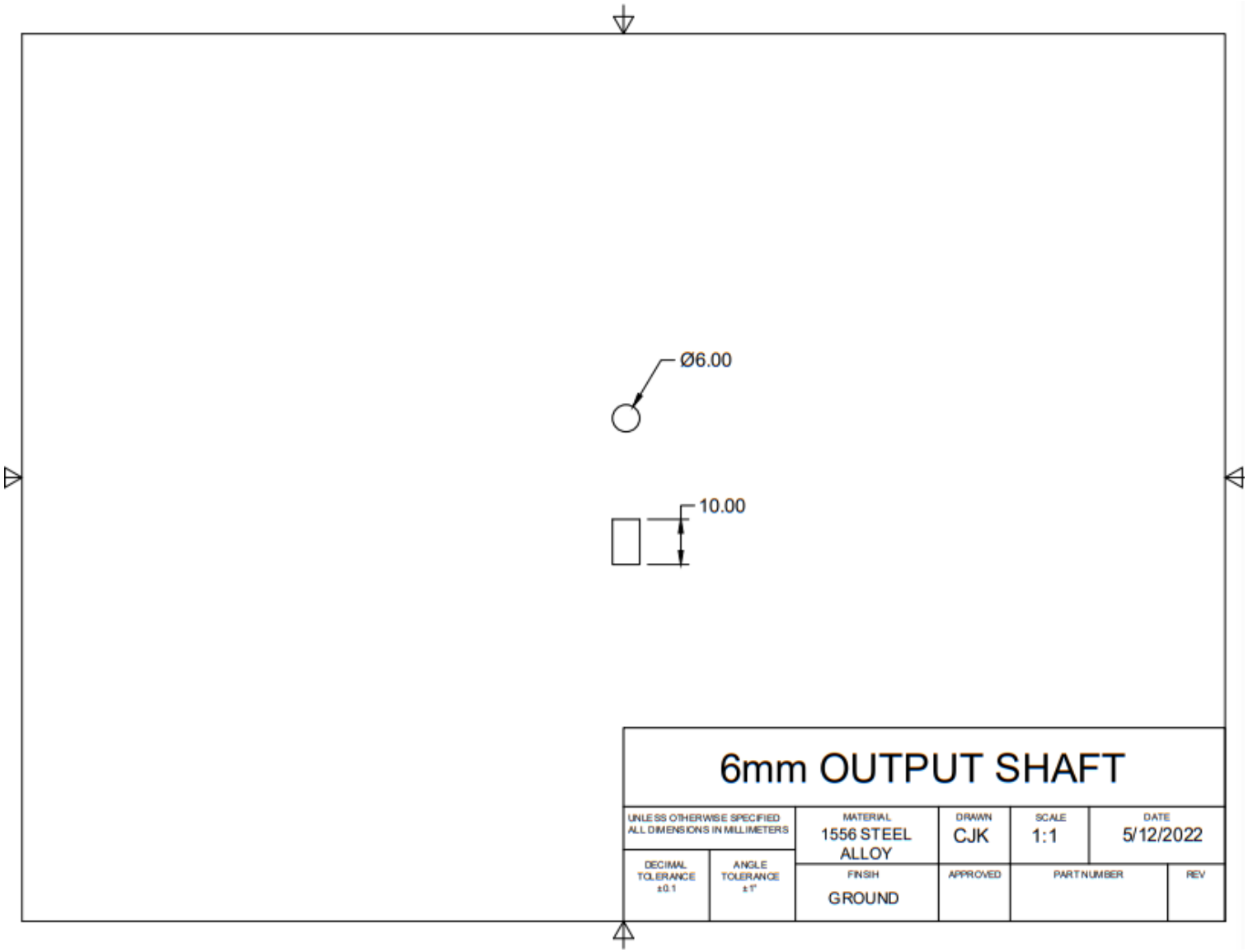
Ø6.00
10.00
6mm OUTPUT SHAFT
UNLESS OTHERWISE SPECIFIED
ALL DIMENSIONS IN MILLIMETERS
MATERIAL
1556 STEEL ALLOY
DRAWN
CJK
SCALE
1:1
DATE
5/12/2022
DECIMAL TOLERANCE
±0.1
ANGLE TOLERANCE
±1°
FINISH
GROUND
APPROVED
PART NUMBER
REV

B: TABLES FOR PLOTS OF FIGURE 9

Phi		Gamma						
radians	deg	x = 0.8	x=0.6	x=0.4	x=0.2	x=0.05	x= 0	x =0.5
0	0	0	0	0	0	0	0	0
0.017	1	0.004	0.012	0.026	0.070	0.319	1.562	0.017
0.035	2	0.009	0.023	0.052	0.138	0.580	1.553	0.035
0.052	3	0.013	0.035	0.078	0.205	0.770	1.545	0.052
0.070	4	0.017	0.046	0.104	0.270	0.903	1.536	0.069
0.087	5	0.022	0.058	0.129	0.331	0.996	1.527	0.087
0.105	6	0.026	0.069	0.154	0.388	1.063	1.518	0.104
0.122	7	0.030	0.081	0.179	0.442	1.113	1.510	0.120
0.140	8	0.035	0.092	0.203	0.492	1.150	1.501	0.137
0.157	9	0.039	0.103	0.226	0.538	1.177	1.492	0.153
0.175	10	0.043	0.114	0.249	0.580	1.198	1.484	0.169
0.192	11	0.047	0.125	0.272	0.618	1.215	1.475	0.185
0.209	12	0.052	0.136	0.293	0.653	1.227	1.466	0.201
0.227	13	0.056	0.146	0.314	0.685	1.236	1.457	0.216
0.244	14	0.060	0.157	0.334	0.713	1.243	1.449	0.231
0.262	15	0.064	0.167	0.354	0.739	1.248	1.440	0.245
0.279	16	0.068	0.177	0.373	0.762	1.251	1.431	0.259
0.297	17	0.072	0.187	0.390	0.783	1.253	1.422	0.273
0.314	18	0.076	0.197	0.408	0.802	1.253	1.414	0.286
0.332	19	0.080	0.206	0.424	0.819	1.253	1.405	0.299
0.349	20	0.084	0.216	0.440	0.834	1.252	1.396	0.312
0.367	21	0.088	0.225	0.455	0.847	1.250	1.388	0.324
0.384	22	0.092	0.234	0.469	0.860	1.248	1.379	0.336
0.401	23	0.095	0.243	0.482	0.870	1.245	1.370	0.347
0.419	24	0.099	0.251	0.495	0.880	1.241	1.361	0.358
0.436	25	0.103	0.259	0.507	0.888	1.237	1.353	0.369
0.454	26	0.106	0.267	0.519	0.895	1.233	1.344	0.379
0.471	27	0.110	0.275	0.530	0.902	1.229	1.335	0.389
0.489	28	0.114	0.283	0.540	0.907	1.224	1.326	0.398
0.506	29	0.117	0.290	0.549	0.912	1.219	1.318	0.407
0.524	30	0.120	0.297	0.558	0.916	1.214	1.309	0.415
0.541	31	0.124	0.304	0.567	0.919	1.208	1.300	0.423
0.559	32	0.127	0.310	0.574	0.922	1.202	1.292	0.431
0.576	33	0.130	0.317	0.582	0.924	1.196	1.283	0.439
0.593	34	0.133	0.323	0.589	0.926	1.190	1.274	0.446
0.611	35	0.136	0.329	0.595	0.927	1.184	1.265	0.452
0.628	36	0.139	0.335	0.601	0.927	1.178	1.257	0.458
0.646	37	0.142	0.340	0.606	0.927	1.171	1.248	0.464

0.663	38	0.145	0.345	0.611	0.927	1.165	1.239	0.470
0.681	39	0.148	0.350	0.616	0.926	1.158	1.230	0.475
0.698	40	0.151	0.355	0.620	0.925	1.151	1.222	0.480
0.716	41	0.153	0.360	0.624	0.924	1.145	1.213	0.485
0.733	42	0.156	0.364	0.627	0.923	1.138	1.204	0.489
0.750	43	0.158	0.368	0.630	0.921	1.131	1.196	0.493
0.768	44	0.161	0.372	0.633	0.918	1.123	1.187	0.497
0.785	45	0.163	0.376	0.635	0.916	1.116	1.178	0.500
0.803	46	0.166	0.379	0.637	0.913	1.109	1.169	0.504
0.820	47	0.168	0.382	0.639	0.910	1.102	1.161	0.507
0.838	48	0.170	0.386	0.640	0.907	1.094	1.152	0.509
0.855	49	0.172	0.388	0.641	0.904	1.087	1.143	0.512
0.873	50	0.174	0.391	0.642	0.901	1.080	1.134	0.514
0.890	51	0.176	0.394	0.643	0.897	1.072	1.126	0.516
0.908	52	0.178	0.396	0.643	0.893	1.064	1.117	0.517
0.925	53	0.180	0.398	0.643	0.889	1.057	1.108	0.519
0.942	54	0.181	0.400	0.643	0.885	1.049	1.100	0.520
0.960	55	0.183	0.402	0.643	0.881	1.042	1.091	0.521
0.977	56	0.185	0.404	0.643	0.876	1.034	1.082	0.522
0.995	57	0.186	0.405	0.642	0.872	1.026	1.073	0.523
1.012	58	0.187	0.406	0.641	0.867	1.018	1.065	0.523
1.030	59	0.189	0.408	0.640	0.862	1.011	1.056	0.524
1.047	60	0.190	0.409	0.639	0.857	1.003	1.047	0.524
1.065	61	0.191	0.409	0.637	0.852	0.995	1.038	0.524
1.082	62	0.192	0.410	0.635	0.847	0.987	1.030	0.523
1.100	63	0.194	0.411	0.634	0.842	0.979	1.021	0.523
1.117	64	0.195	0.411	0.632	0.836	0.971	1.012	0.522
1.134	65	0.195	0.411	0.630	0.831	0.963	1.004	0.522
1.152	66	0.196	0.412	0.627	0.825	0.955	0.995	0.521
1.169	67	0.197	0.411	0.625	0.820	0.947	0.986	0.520
1.187	68	0.198	0.411	0.622	0.814	0.939	0.977	0.518
1.204	69	0.198	0.411	0.620	0.808	0.931	0.969	0.517
1.222	70	0.199	0.411	0.617	0.803	0.923	0.960	0.516
1.239	71	0.200	0.410	0.614	0.797	0.915	0.951	0.514
1.257	72	0.200	0.410	0.611	0.791	0.907	0.942	0.512
1.274	73	0.200	0.409	0.608	0.785	0.899	0.934	0.511
1.292	74	0.201	0.408	0.605	0.779	0.891	0.925	0.509
1.309	75	0.201	0.407	0.601	0.772	0.883	0.916	0.506
1.326	76	0.201	0.406	0.598	0.766	0.875	0.908	0.504
1.344	77	0.201	0.405	0.594	0.760	0.867	0.899	0.502
1.361	78	0.201	0.403	0.591	0.754	0.858	0.890	0.500
1.379	79	0.201	0.402	0.587	0.747	0.850	0.881	0.497
1.396	80	0.201	0.400	0.583	0.741	0.842	0.873	0.495

1.414	81	0.201	0.399	0.579	0.735	0.834	0.864	0.492
1.431	82	0.201	0.397	0.575	0.728	0.826	0.855	0.489
1.449	83	0.201	0.395	0.571	0.722	0.818	0.846	0.486
1.466	84	0.200	0.394	0.567	0.715	0.809	0.838	0.483
1.484	85	0.200	0.392	0.563	0.708	0.801	0.829	0.480
1.501	86	0.200	0.390	0.558	0.702	0.793	0.820	0.477
1.518	87	0.199	0.387	0.554	0.695	0.785	0.812	0.474
1.536	88	0.199	0.385	0.550	0.688	0.776	0.803	0.470
1.553	89	0.198	0.383	0.545	0.682	0.768	0.794	0.467
1.571	90	0.197	0.381	0.540	0.675	0.760	0.785	0.464
1.588	91	0.197	0.378	0.536	0.668	0.751	0.777	0.460
1.606	92	0.196	0.376	0.531	0.661	0.743	0.768	0.457
1.623	93	0.195	0.373	0.526	0.654	0.735	0.759	0.453
1.641	94	0.194	0.370	0.521	0.647	0.727	0.750	0.449
1.658	95	0.193	0.368	0.517	0.640	0.718	0.742	0.445
1.676	96	0.192	0.365	0.512	0.633	0.710	0.733	0.441
1.693	97	0.191	0.362	0.507	0.626	0.702	0.724	0.438
1.710	98	0.190	0.359	0.502	0.619	0.693	0.716	0.434
1.728	99	0.189	0.356	0.496	0.612	0.685	0.707	0.430
1.745	100	0.188	0.353	0.491	0.605	0.677	0.698	0.425
1.763	101	0.187	0.350	0.486	0.598	0.668	0.689	0.421
1.780	102	0.186	0.347	0.481	0.591	0.660	0.681	0.417
1.798	103	0.184	0.343	0.476	0.584	0.652	0.672	0.413
1.815	104	0.183	0.340	0.470	0.577	0.643	0.663	0.408
1.833	105	0.182	0.337	0.465	0.569	0.635	0.654	0.404
1.850	106	0.180	0.333	0.460	0.562	0.626	0.646	0.400
1.868	107	0.179	0.330	0.454	0.555	0.618	0.637	0.395
1.885	108	0.177	0.326	0.449	0.548	0.610	0.628	0.391
1.902	109	0.176	0.323	0.443	0.541	0.601	0.620	0.386
1.920	110	0.174	0.319	0.438	0.533	0.593	0.611	0.382
1.937	111	0.172	0.316	0.432	0.526	0.585	0.602	0.377
1.955	112	0.171	0.312	0.426	0.519	0.576	0.593	0.372
1.972	113	0.169	0.308	0.421	0.511	0.568	0.585	0.368
1.990	114	0.167	0.305	0.415	0.504	0.559	0.576	0.363
2.007	115	0.166	0.301	0.409	0.497	0.551	0.567	0.358
2.025	116	0.164	0.297	0.404	0.489	0.542	0.559	0.353
2.042	117	0.162	0.293	0.398	0.482	0.534	0.550	0.348
2.059	118	0.160	0.289	0.392	0.474	0.526	0.541	0.343
2.077	119	0.158	0.285	0.386	0.467	0.517	0.532	0.338
2.094	120	0.156	0.281	0.380	0.460	0.509	0.524	0.333
2.112	121	0.154	0.277	0.374	0.452	0.500	0.515	0.328
2.129	122	0.152	0.273	0.368	0.445	0.492	0.506	0.323
2.147	123	0.150	0.269	0.363	0.437	0.483	0.497	0.318

2.164	124	0.148	0.265	0.357	0.430	0.475	0.489	0.313
2.182	125	0.146	0.260	0.351	0.422	0.467	0.480	0.308
2.199	126	0.144	0.256	0.345	0.415	0.458	0.471	0.303
2.217	127	0.142	0.252	0.339	0.407	0.450	0.463	0.298
2.234	128	0.139	0.248	0.332	0.400	0.441	0.454	0.293
2.251	129	0.137	0.243	0.326	0.392	0.433	0.445	0.287
2.269	130	0.135	0.239	0.320	0.385	0.424	0.436	0.282
2.286	131	0.133	0.235	0.314	0.377	0.416	0.428	0.277
2.304	132	0.130	0.230	0.308	0.369	0.407	0.419	0.272
2.321	133	0.128	0.226	0.302	0.362	0.399	0.410	0.266
2.339	134	0.126	0.221	0.296	0.354	0.391	0.401	0.261
2.356	135	0.123	0.217	0.290	0.347	0.382	0.393	0.255
2.374	136	0.121	0.213	0.283	0.339	0.374	0.384	0.250
2.391	137	0.118	0.208	0.277	0.332	0.365	0.375	0.245
2.409	138	0.116	0.203	0.271	0.324	0.357	0.367	0.239
2.426	139	0.114	0.199	0.265	0.316	0.348	0.358	0.234
2.443	140	0.111	0.194	0.258	0.309	0.340	0.349	0.228
2.461	141	0.109	0.190	0.252	0.301	0.331	0.340	0.223
2.478	142	0.106	0.185	0.246	0.293	0.323	0.332	0.217
2.496	143	0.103	0.180	0.239	0.286	0.314	0.323	0.212
2.513	144	0.101	0.176	0.233	0.278	0.306	0.314	0.206
2.531	145	0.098	0.171	0.227	0.270	0.297	0.305	0.201
2.548	146	0.096	0.166	0.220	0.263	0.289	0.297	0.195
2.566	147	0.093	0.162	0.214	0.255	0.280	0.288	0.190
2.583	148	0.090	0.157	0.208	0.247	0.272	0.279	0.184
2.601	149	0.088	0.152	0.201	0.240	0.263	0.271	0.178
2.618	150	0.085	0.147	0.195	0.232	0.255	0.262	0.173
2.635	151	0.082	0.143	0.189	0.224	0.246	0.253	0.167
2.653	152	0.080	0.138	0.182	0.217	0.238	0.244	0.161
2.670	153	0.077	0.133	0.176	0.209	0.229	0.236	0.156
2.688	154	0.074	0.128	0.169	0.201	0.221	0.227	0.150
2.705	155	0.071	0.123	0.163	0.194	0.212	0.218	0.144
2.723	156	0.069	0.119	0.156	0.186	0.204	0.209	0.139
2.740	157	0.066	0.114	0.150	0.178	0.195	0.201	0.133
2.758	158	0.063	0.109	0.143	0.170	0.187	0.192	0.127
2.775	159	0.060	0.104	0.137	0.163	0.179	0.183	0.122
2.793	160	0.058	0.099	0.130	0.155	0.170	0.175	0.116
2.810	161	0.055	0.094	0.124	0.147	0.162	0.166	0.110
2.827	162	0.052	0.089	0.118	0.139	0.153	0.157	0.104
2.845	163	0.049	0.084	0.111	0.132	0.145	0.148	0.099
2.862	164	0.046	0.079	0.105	0.124	0.136	0.140	0.093
2.880	165	0.043	0.075	0.098	0.116	0.128	0.131	0.087
2.897	166	0.040	0.070	0.091	0.109	0.119	0.122	0.081

2.915	167	0.038	0.065	0.085	0.101	0.111	0.113	0.075
2.932	168	0.035	0.060	0.078	0.093	0.102	0.105	0.070
2.950	169	0.032	0.055	0.072	0.085	0.094	0.096	0.064
2.967	170	0.029	0.050	0.065	0.078	0.085	0.087	0.058
2.985	171	0.026	0.045	0.059	0.070	0.077	0.079	0.052
3.002	172	0.023	0.040	0.052	0.062	0.068	0.070	0.047
3.019	173	0.020	0.035	0.046	0.054	0.060	0.061	0.041
3.037	174	0.017	0.030	0.039	0.047	0.051	0.052	0.035
3.054	175	0.015	0.025	0.033	0.039	0.043	0.044	0.029
3.072	176	0.012	0.020	0.026	0.031	0.034	0.035	0.023
3.089	177	0.009	0.015	0.020	0.023	0.026	0.026	0.017
3.107	178	0.006	0.010	0.013	0.016	0.017	0.017	0.012
3.124	179	0.003	0.005	0.007	0.008	0.009	0.009	0.006
3.142	180	2E-17	3.5E-17	4.6E-17	5.4E-17	6E-17	6.1E-17	4.1E-17

C: TABLE USED FOR PLOT IN FIGURE 19

Z4	11	pins
M1	1	Nm
K1	1	
Z3	10	lobes
r2	0.0385	m
Px	14.28571	N

phi	phi rad	Py 1	Py 2	Py 3	Py 4	Py 5	Sum Py	P
15	0.26	-4.304	1.681	2.257	1.614	0.656	1.904	14.412
16	0.28	-4.863	1.625	2.264	1.642	0.683	1.352	14.350
17	0.30	-5.491	1.567	2.270	1.670	0.711	0.727	14.304
18	0.31	-6.203	1.505	2.274	1.697	0.740	0.012	14.286
19	0.33	-7.017	1.439	2.277	1.724	0.768	-0.809	14.309
20	0.35	-7.957	1.369	2.279	1.750	0.797	-1.762	14.394
21	0.37	-9.054	1.294	2.280	1.777	0.826	-2.877	14.573
22	0.38	-10.353	1.216	2.280	1.802	0.855	-4.200	14.890
23	0.40	-11.916	1.132	2.278	1.828	0.884	-5.793	15.416
24	0.42	-13.832	1.044	2.275	1.852	0.913	-7.747	16.251
25	0.44	-16.240	0.951	2.271	1.877	0.943	-10.198	17.552
26	0.45	-19.357	0.851	2.265	1.901	0.973	-13.367	19.564
27	0.47	-23.555	0.746	2.258	1.924	1.002	-17.624	22.687
28	0.49	-29.520	0.634	2.249	1.947	1.032	-23.657	27.636
29	0.51	-38.673	0.516	2.239	1.970	1.062	-32.886	35.855
30	0.52	-54.519	0.390	2.227	1.991	1.092	-48.818	50.866
31	0.54	-88.684	0.256	2.214	2.012	1.122	-83.080	84.299
32	0.56	-216.730	0.113	2.199	2.033	1.152	-211.233	211.715
33	0.58	594.021	-0.039	2.182	2.053	1.182	599.399	599.570
34	0.59	130.690	-0.201	2.163	2.072	1.212	135.936	136.685
35	0.61	75.064	-0.375	2.142	2.091	1.242	80.164	81.427
36	0.63	53.412	-0.560	2.120	2.109	1.272	58.353	60.076
37	0.65	41.881	-0.759	2.095	2.126	1.302	46.645	48.784
38	0.66	34.711	-0.973	2.068	2.142	1.332	39.281	41.798
39	0.68	29.817	-1.203	2.039	2.158	1.362	34.173	37.039
40	0.70	26.259	-1.451	2.008	2.173	1.391	30.380	33.571
41	0.72	23.552	-1.720	1.975	2.187	1.421	27.415	30.914
42	0.73	21.422	-2.011	1.939	2.200	1.450	24.999	28.793
43	0.75	19.699	-2.328	1.900	2.212	1.479	22.962	27.043
44	0.77	18.275	-2.675	1.859	2.224	1.508	21.191	25.557
45	0.79	17.076	-3.055	1.815	2.234	1.537	19.608	24.261

D: LINKS TO CAD FILES

https://gallery.autodesk.com/projects/169363/craig-kimball-101-cycloidal-gearbox-actuator-for-cal-poly-legged-robotics-platform